Aerodynamic Properties of the Inboard Wing Concept

Matthew W. Orr

Thesis submitted to the Faculty of the Virginia Polytechnic Institute and State University in partial fulfillment of the requirements for the degree of

Master of Science
in
Aerospace Engineering

Joseph A. Schetz, Chair
William Mason
James F. Marchman III

September 19, 2000

Blacksburg, Virginia

Keywords: inboard wing, configuration testing, aerodynamics

Aerodynamic Properties of the Inboard Wing Concept

Matthew W. Orr

(Abstract)

This investigation examines a new concept in airliner configurations from an experimental aerodynamics point of view. The concept proposes mounting the fuselages at the tips of a low aspect ratio wing. The motivation for this configuration is to provide an increase in the number of passengers carried with no increase in span over conventional designs. An additional motivation is the change in the wake flow of the wing, due to the fuselages and vertical tails, which may reduce the effect of the trailing vortex on trailing aircraft. During this investigation, two models of different scales were used to measure the aerodynamic forces and moments of the inboard wing configuration. The tests were conducted in the Virginia Tech 6X6 ft. wind tunnel using a six-component strain gauge balance. The Reynolds number based on chord for the small model was 465,000 and for the large model was 1,225,000. For reference, tests were also conducted with a plain wing having the same span as the full configuration. The *L/D* values found for this non-optimized configuration were modest compared to those for conventional transports. The vertical tails were shown to act as winglets, reducing drag and increasing *L/D*. These results suggest areas for substantial improvement in aerodynamic performance of the configuration.

Acknowledgments

I appreciate the guidance and insightful advice from Dr. Schetz, my advisor in this research. The aid of James Bamba with construction of the models and Samantha Magill with testing proved invaluable. The comments of Drs. Marchman and Mason were valuable in the planning and execution of these tests. I would also like to thank Scott Gallimore for his insightful comments on this paper.

Table of Contents

List of Figures

Nomenclature

α	Angle of Attack
$\overline{C}$	Mean Aerodynamic Chord (4.6in. small, 22.3in. large model)
$C_D = \frac{Drag}{qS_{ref}}$	Drag Coefficient
C_{Do}	Zero Lift Drag Coefficient
$C_L = \frac{Lift}{qS_{ref}}$	Lift Coefficient
$C_M = \frac{Moment}{qS_{ref}\overline{C}}$	Pitching Moment Coefficient
$L/D = \frac{Lift}{Drag}$	Lift to Drag Ratio
L/D_{max}	Maximum Lift to Drag ratio
$R_e = \frac{\rho V \overline{C}}{\mu}$	Reynolds Number
$q = 1/2\rho V^2$	Dynamic Pressure
S_{ref}	Reference Wing Area (0.298 ft^2 small model, 6.91 ft^2 large model)
T	Tunnel Temperature
X_{ref}	Moment Reference Location (10% $\overline{C}$)
ρ	Air Density
V	Flow Velocity
μ	Dynamic Viscosity of Air

Introduction

The inboard wing configuration has two fuselages mounted on the tips of a low aspect ratio wing. M. L. Spearman (Spearman, 1997 and 1998) first proposed this configuration. Providing an increase in the number of passengers carried with no increase in span over conventional designs is the underlying motivation for this configuration. The inboard wing concept will allow an increase in payload capacity while the span is held fixed, and maintaining current span limits would allow the use of present airports. Possible structural benefits may also be realized, as the wing thickness would be high and the span fairly low for a given payload capacity. Another motivation is a possible reduction in the intensity of the wing wake due to the interaction of fuselages and vertical tails. This may reduce the effect of the tip vortices on trailing aircraft, as well as providing a possible reduction in induced drag.

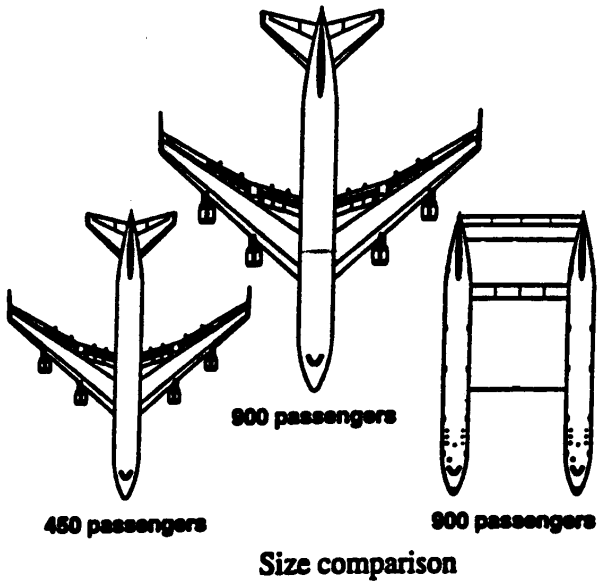

Figure 1: Inboard Wing Airliner Concept (Spearman 1998)

One of the concepts proposed by Spearman (1998) is shown in figure 1. This concept proposes mating existing fuselages from a conventional airliner to form an aircraft with a much higher passenger capacity. This figure shows what a possible aircraft might look like if two Boeing 747 fuselages are mated with an inboard wing. The aircraft would have a passenger capacity of up to 900 people and the thickness to chord

ratio could be quite high. This may allow a 10-12 percent thick wing, facilitating submerging the engines in the wing. A conventional 747 along with a conventional aircraft sized to hold 900 passengers are shown. This clearly demonstrates the smaller span of the inboard wing configuration when large passenger capacities are required.

This investigation is designed to provide basic aerodynamic information about the inboard-wing configuration. Experimental force and moment data give the basic characteristics of the configuration and provide a basis for validating computational results. The tests were performed in the Virginia Tech 6X6 ft. Stability Wind Tunnel. The maximum Reynolds number approached two million in these tests. The large six-foot square cross section and twenty-four foot long test section allowed the flow visualization to be performed several chord lengths behind the model while providing excellent flow quality.

Previous tests on this configuration (Spearman, 1998) used a similar model. The basic configuration consists of two cylindrical fuselages with rounded noses and tail cones mounted to a wing that has an aspect ratio of two (see Figure 2). A vertical tail is affixed to the end of each fuselage. The horizontal tail was mounted on the tips of the vertical tail for the tests performed by Spearman. The tail placement on the models used for this series of tests is on the centerline of the fuselages. This configuration is not optimized for maximum performance and is simply a generic representation of a possible arrangement. The maximum Reynolds number obtained in the previous tests was roughly 600,000.

Two models were used in the new experiments. A large, 22.27 inch chord, model and a smaller, 4.63 inch chord, model were used. The use of the small model allowed for a large angle of attack range during force tests that couldn't be reached with the large model due to balance limits. This model also permitted mounting in the front of the test section, which allowed far-field wake visualization with a tuft grid.

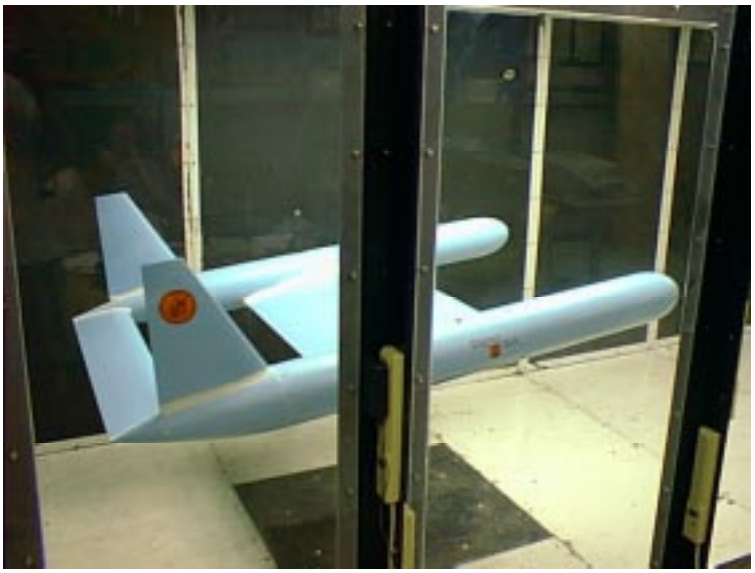

Figure 2: Large Model in Stability Tunnel

A strain gauge balance was used to collect the force and moment data of the configuration. The force measurements were made at the following flow conditions;

Velocity (fps)	q (psf)	q (inches of water)	Re (Small Model)	Re (Large Model)
122	15.6	3	255,000	1,225,000
173	31.2	6	360,000	1,733,000
223	52	10	465,000	N/A

The balance limits constrained the angles of attack (AOA) for which moment data for the large model could be obtained. The large model was tested at 3 inches of water for moment measurements. Some force measurements were made at 6 inches of water so that a higher Reynolds number could be obtained to determine if there was a significant Reynolds number dependence in the results. A dummy moment head was used to obtain these results and this is compared to the moment head in Figure3.

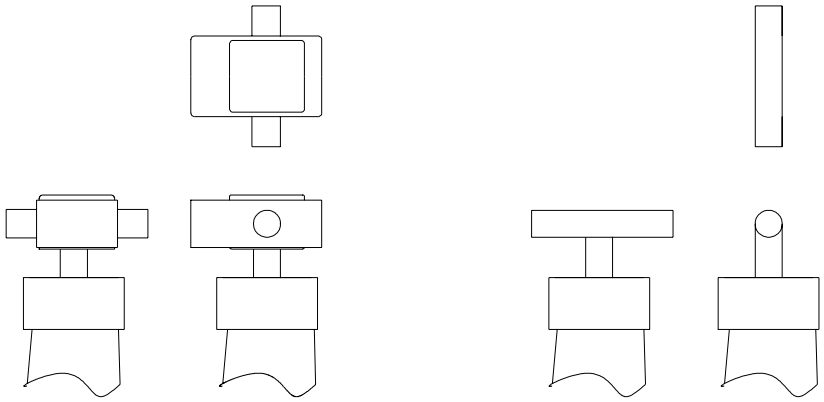

Figure 3: Moment Head (on left) and Dummy Moment Head (on Right)

Tufts, both on the model and in a grid, allowed photographs to be taken that show general trends in the flow. These grids also aided in determining the approximate location of the wing and vertical tail vortices. Flow visualization tests were run at lower dynamic pressures (0.5 (2.6 psf) to 1.5 (7.8 psf) inches of water) so that the tufts would not depart the model. Video and still photographs were taken to document the tests and show the behavior of the tufts in the flow.

In conjunction with the experiments, a vortex lattice method code was used to complement results. The code was VLM4.997, and it was used to predict the lift curve slope of the wing-body combination. This served to aid in validating the experimental data and flow corrections for the tunnel walls.

Models

Small Model

The general arrangement of the small model is shown in Figure 4. The fuselages were constructed out of PVC pipe. Carved foam was used for the nose and tail cones and the small model had a carved basswood wing that used a metal spar for reinforcement and to attach the model to the balance. The wing and fuselages were permanently affixed and could not be separated. The horizontal tail incidence angle could be changed. The vertical tails also had a variable geometry arrangement. The airfoil used for the main wings, on both models, was the NACA 23012. All of the tail sections used the NACA 0012 airfoil section. These airfoils were chosen as they where used in previous tests of this configuration (Spearman, 1998).

During these tests the vertical and horizontal tail settings of the small model were set at a zero degrees relative to the centerline of the fuselages. The vertical and horizontal tail could be removed so that the effects of the configuration changes on the force and moment data could be explored. The wing span was defined as going from the outer edge of the right fuselage to the outer edge of the left fuselage and was 9.27 inches. The resulting wing area, used in data reduction, was 0.298 square feet. All of the moment data is referenced to the 10% chord location on both the large and small models.

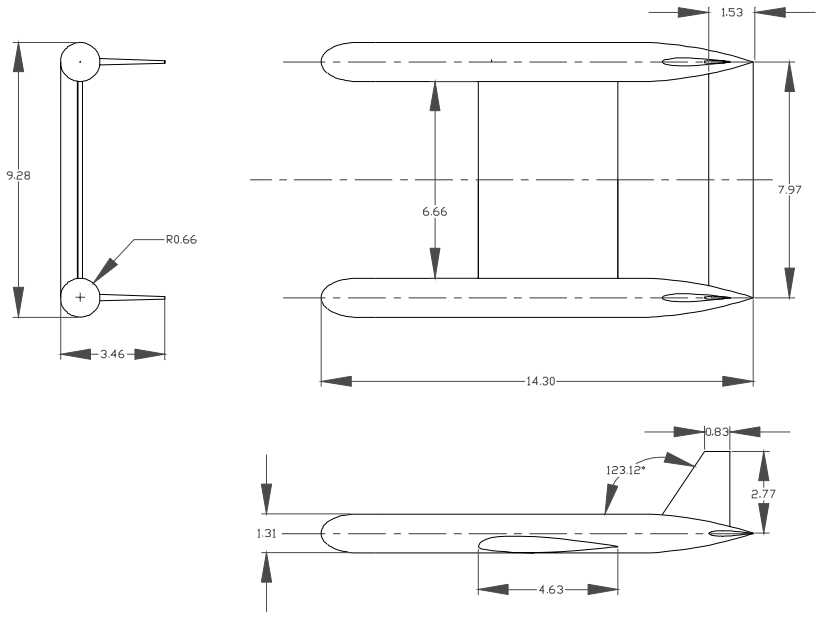

Figure 4: Small Model (All Dimensions in Inches)

Figure 5 shows the small model on a mount that was constructed to allow the model to be positioned near the front of the test section. This arrangement allowed flow visualization using a tuft grid to be performed at 20-30 feet behind the model. This compares with a maximum downstream distance of ten feet when the model was mounted on the force balance.

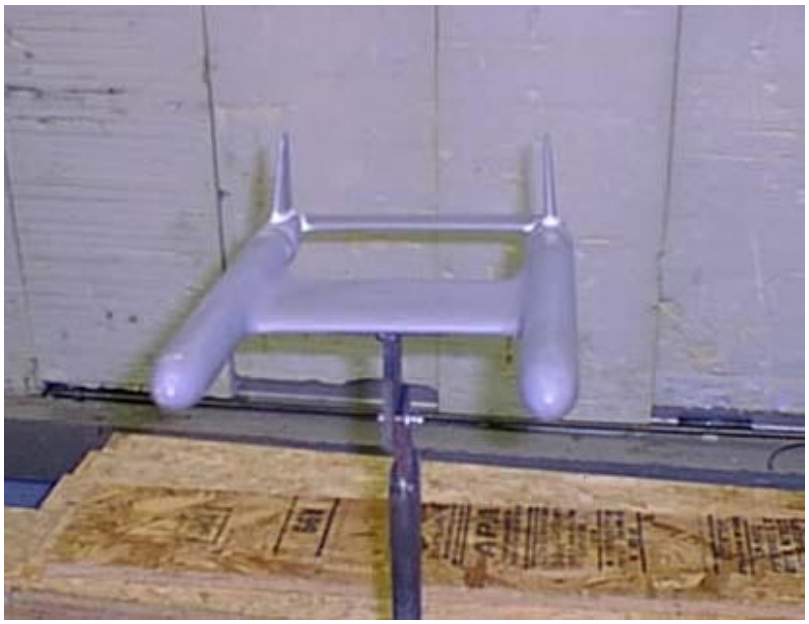

Figure 5: Small Model

Large Model

Figure 2 shows the large model in the test section of the Stability Wind Tunnel in the fully assembled configuration. This model has a 44.66-inch span and a 22.27-inch chord. The reference span was to the outer edges of the fuselages, and the resulting reference area is 6.91 square feet. These values were used for all of the data reduction and subsequent calculations. The pitching moment was referenced to the 10% chord location on the large model.

Figure 6 is the AutoCAD drawing used to construct the large model. The figure has all dimensions in inches. The wing of the model was constructed using foam cores to form the NACA 23012 airfoil section. The airfoil was then sheeted with 1/64-inch plywood skins and it utilized balsa wood leading edges. The shaded areas in Figure 6 show the structure of the model including the large aluminum plate that runs through the center of the wing. This provides a solid location for mounting the model on the moment head in the tunnel. The plate also provides a ridged mount for attaching the fuselages.

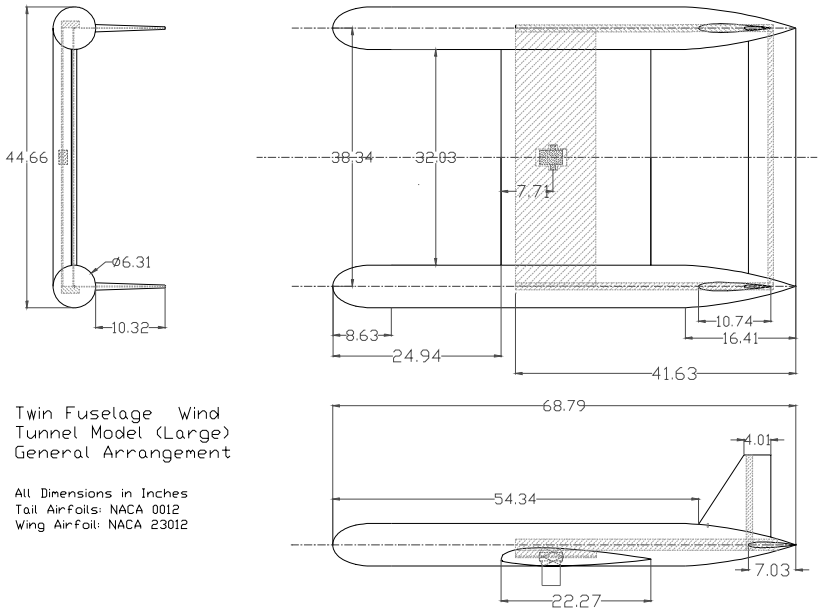

Figure 6: Large Model Layout Drawing (All Dimensions in Inches)

The horizontal and vertical tails were constructed in the same manner as the wing except they used steel rods for mounting and reinforcement. The fuselages consist of two 6.31-inch diameter plastic pipes with internal reinforcement and wooden nose and tail cones. These construction methods allowed the models to be completed with reasonable accuracy in a very short period of time. The airfoil section on the wing of the large model was measured and is compared to the actual coordinates in Figure 7.

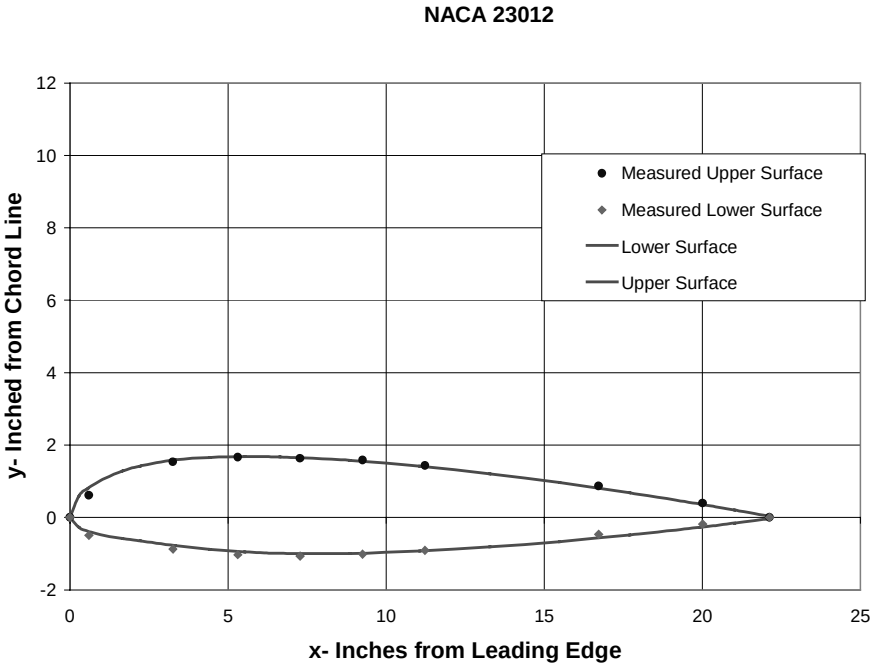

Figure 7: Large Model Airfoil Coordinate Check

No transition tripping was employed on either model. This was not done, as the Reynolds number was high on the large model. Another reason transition strips were not used was that a purpose of this investigation was to examine the effects of Reynolds number on the results. Some attempts were made to use transition strips on the small model but the thickness of the strips used was to great for the small size of the model.

Facility and Instrumentation

Wind Tunnel

The Virginia Tech Stability Wind Tunnel is a continuous single return subsonic wind tunnel with a 24-foot long test section that has a 6X6 foot square cross section. The general design layout is illustrated in Figure 8. A 600-hp D.C. motor driving a 14-foot propeller powers the tunnel. The propeller provides a maximum speed of 275 fps and a Reynolds number per foot up to 1,660,000 in a normal 6X6 foot configuration.

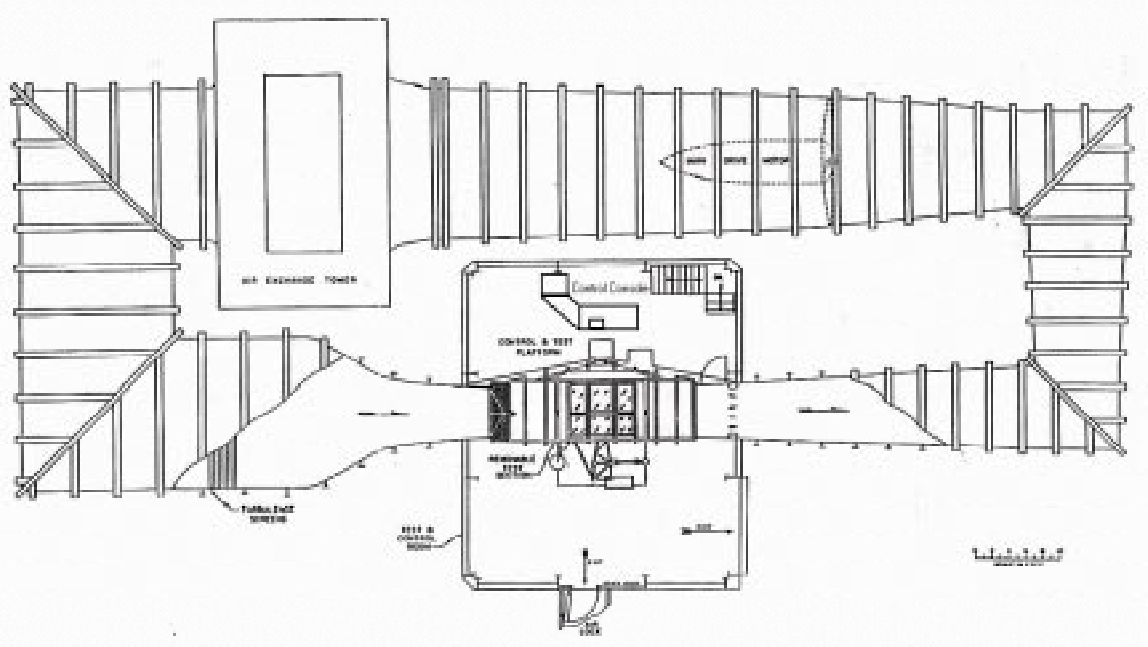

Figure 8: Virginia Tech Stability Tunnel Layout

Force and Moment Data

The three component SR-1 strut balance was used to measure all forces recorded during these tests. The STO-3M moment head, a three-moment strain gauge balance, was mounted on top of the strut balance to collect moment data. The model was attached to mounting posts on the balance. The following table displays the balance limits.

	SR-1 Force Balance
Normal Force (lb)	200
Axial Force (lb)	100
Side Force (lb)	100
	STOM-3 Moment Head
Pitching Moment (in-lb)	200
Rolling Moment (in-lb)	300
Yawing Moment (in-lb)	200

The data acquisition (DAQ) system used Measurements Group 2310 Signal Conditioning Amplifiers that fed the signal into a National Instruments AT-MIO-16-XE-10 DAQ Card mounted in a personal computer. LabView 4.0 was used as the PC to DAQ system interface program in a Windows 95 environment. The basic data reduction was performed automatically. This system allowed the operator of the tunnel to monitor the data as it was acquired, reduce the data, and then record the data to a file for future use all in one step.

The operator first took a tare reading with the models sitting on the balance before the start of each test. The tunnel was then set to the desired dynamic pressure manually. Then, each data point was acquired using the DAQ system. The voltages of all the sensors, in addition to reduced data, were recorded in a file and stored on the local hard drive of the computer.

The small model used an automatic angle of attack changing device so that sweeps though a wide range of angles of attack could be accomplished in a very short period of time. This apparatus dictated the model size, as it is limited in capacity.

The large model was mounted directly to the moment head. This necessitated changing the model's angle of attack by hand. To do this, the model data was acquired at a particular angle of attack, the tunnel was then shut off, and the angle of attack of the large model was changed. Even with this testing method the moment head limits on the balance could be exceeded at an angle of attack of about six degrees. To get a higher angle of attack range a "dummy moment head" was constructed. This consisted of a welded steel "T" (see Figure 3). This allowed a larger range of force measurements to be made at higher Reynolds numbers were the moment head limits would have been exceeded.

Force and Moment Results

The following sections describe the force and moment coefficient results obtained for the large and small models. The results follow the same general format for the sections on the large and small model. First, the effect of changing the Reynolds number is shown. Then, the effect of changing the model configuration is shown. The third section compares the large and small model results.

Small Model Results

Figure 9 shows the effects of Reynolds number on the lift curve slope and of the stall behavior on the small model. The model had only the wing and bodies attached during these tests. There is a slight variation in the behavior of the wing body combination near stall when the Reynolds number was changed. The lift curve slope remained consistent throughout the range of Reynolds numbers tested, approximately 255,000 to 465,000. This Reynolds number regime was considered sufficient to investigate as it and any major changes in the data should be evident. Stall hysteresis loops were investigated, and there appears to be some non-linearity in the data. The arrows on the curves indicate the path over which the data was taken. The model must be brought to a lower angle of attack for it to reattach than it must be to attain stall. Appendix 1 contains a summary of data taken for the angle of attack device and balance without the model affixed. Those figures show acceptably low tare values for these experiments.

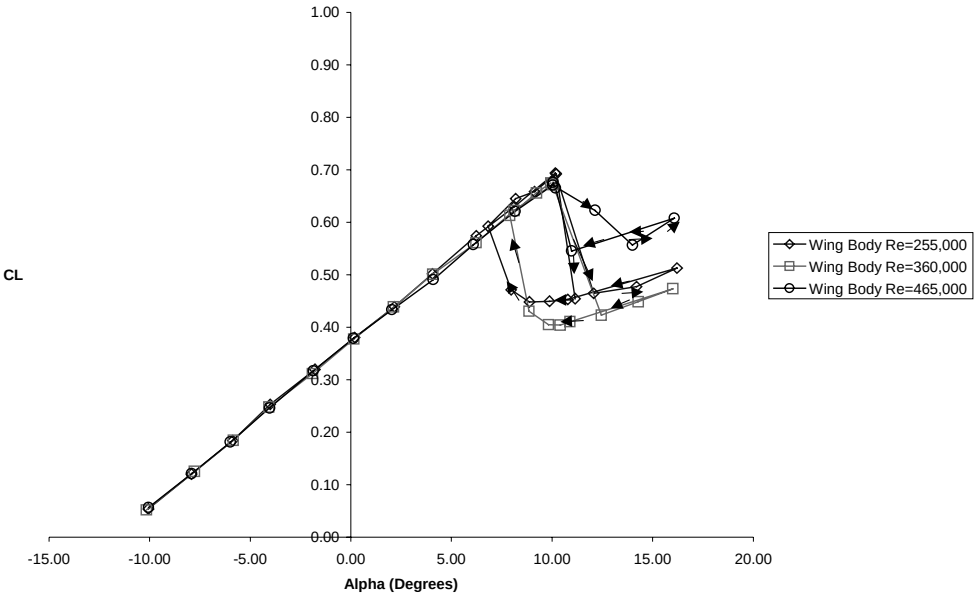

Figure 9: Small Model C_L vs. α at Different Reynolds Numbers (Angle of Attack Referenced to Body Centerline)

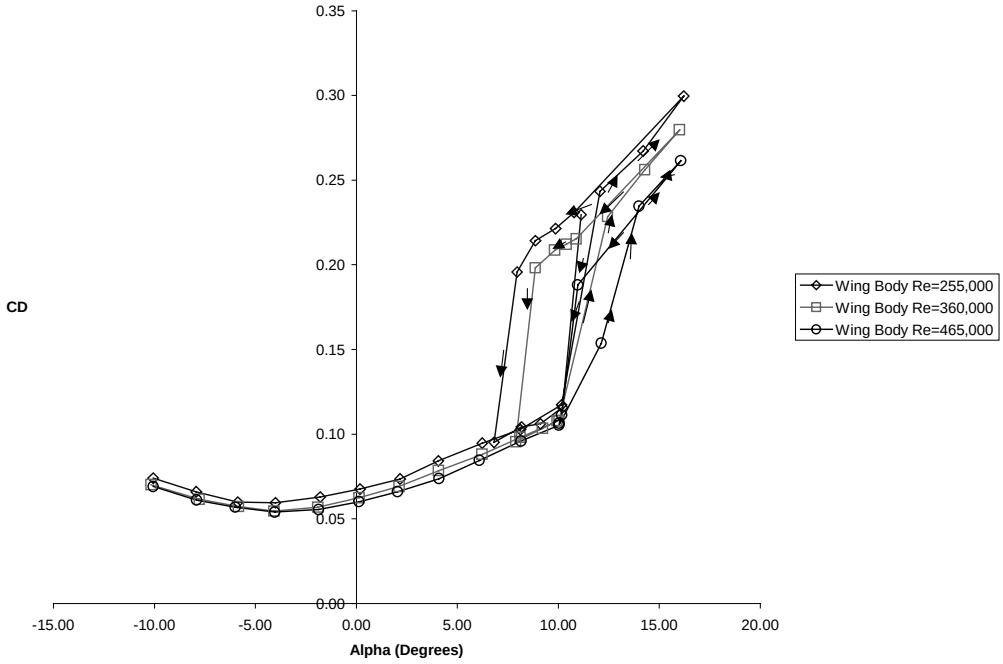

Figure 10: Small Model C_D vs. α at Different Reynolds Numbers (Angle of Attack Referenced to Body Centerline)

There is some Reynolds number dependence evident in the drag data for the small model as shown in Figure 10. As *Re* increases, the drag decreases slightly throughout the range of measurement where the model was not stalled. This indicates that the results for the small model are dependent on Reynolds number. When stall occurs, the small model shows stall hysteresis in the drag coefficient data.

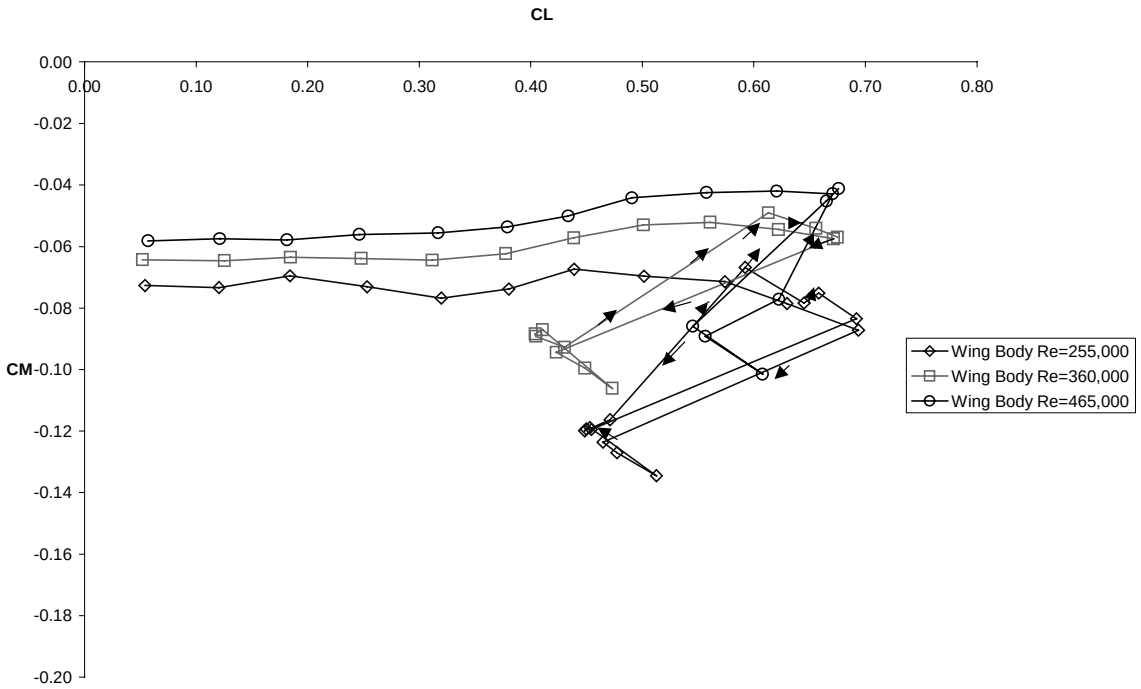

Figure 11: Small Model C_M vs. C_L at Different Reynolds Numbers (X_{ref}=10%$\overline{C}$)

The pitching moment data also exhibits a dependence on Reynolds number as shown in Figure 11. The flat moment curves indicate that the aerodynamic center is close to the chosen reference point of 10%$\overline{C}$. This corresponds to a X_{ref} position of 0.463 inches from the leading edge of the model. The higher the Reynolds number, the smoother the data appears. In the case when the Reynolds number is equal to 255,000, there are bumps in the curve around a C_L of 0.2 and again at 0.5. There also is a second hysteresis loop rather than the single one shown in the lift and drag data. The main effect

of changing Reynolds number is the change in the zero lift pitching moment of the model.

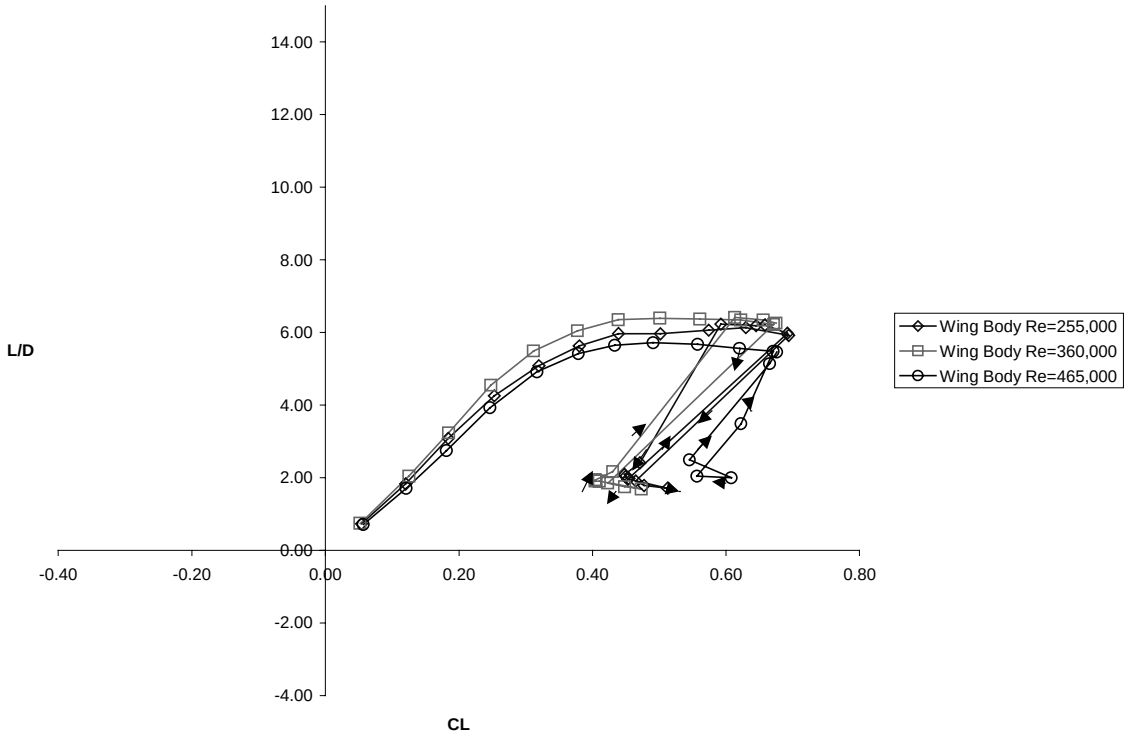

Figure 12: Small Model *L/D* vs. C_L at Different Reynolds Numbers

The lift-drag ratio increases with increasing Reynolds number. This data is shown in Figure 12. The maximum value of *L/D* for the wing body combination is 6.4 at a Reynolds number of 465,000, and the maximum *L/D* is found at a C_L of about 0.45. The lowest value of L/D_{max} is found for the lowest Reynolds number case.

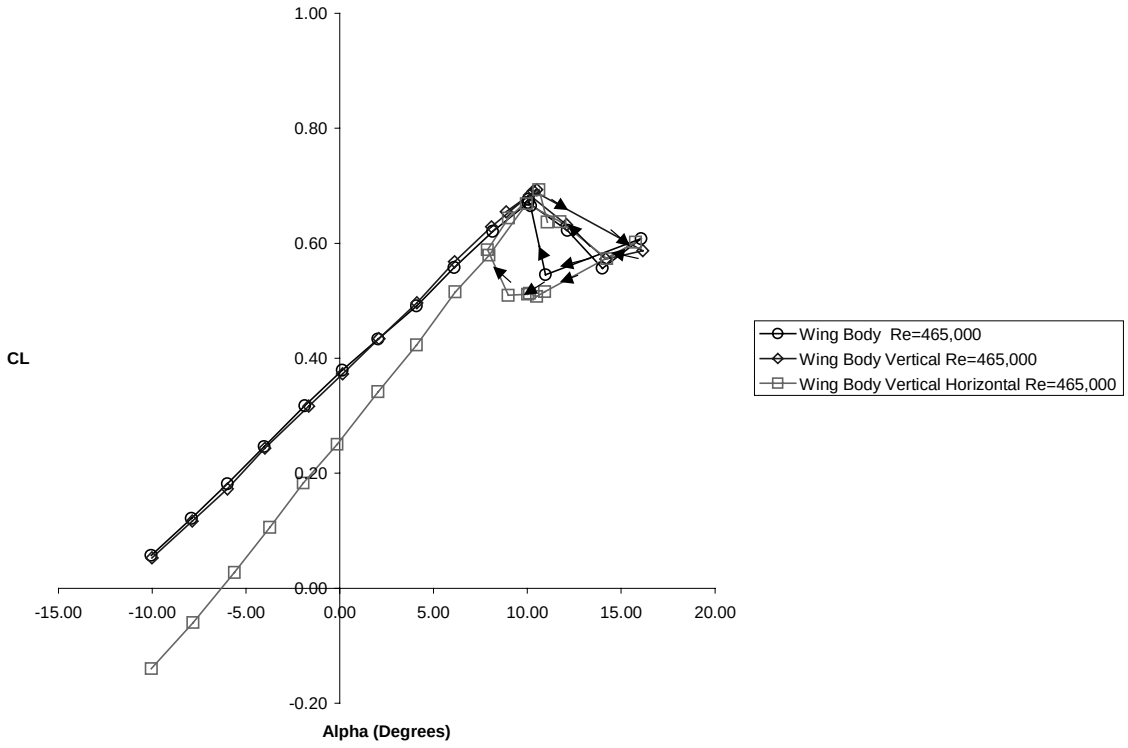

Figure 13: Small Model C_L vs. α with Configuration Changes (Angle of Attack Referenced to Body Centerline)

Figure 13 shows the effects of model configuration on the lift curve slope for the small model. This result suggests that possible further increases in the maximum C_L could be achieved with care paid to the geometry and design of the vertical tails. The addition of the horizontal tail increases the lift curve slope and changes the zero lift angle of attack five degrees. This large shift is an indication that the horizontal tail has a large download on it. This indicates that the horizontal tail may have had a slight misalignment with the fuselages as a large positive pitching moments is shown in Figure 15.

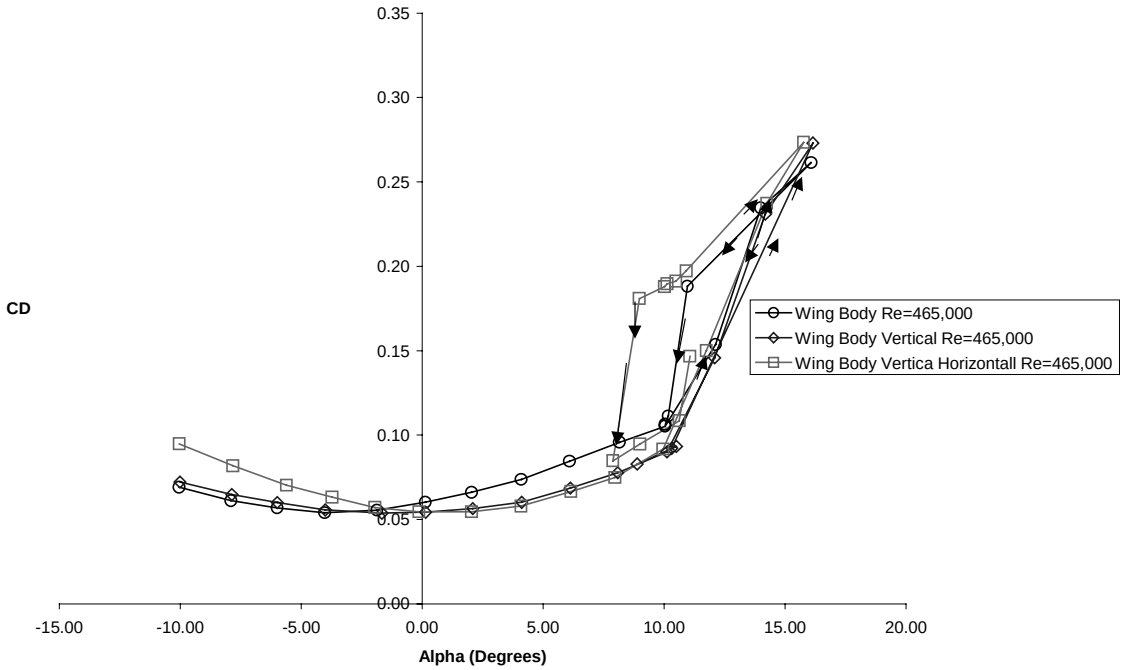

Figure 14: Small Model C_D vs. α with Configuration Changes (Angle of Attack Referenced to Body Centerline)

Figure 14 shows the effects of the model configuration on the drag data. The drag decreases in some areas when the vertical tails are added, but this effect is only consistent above an angle of attack of –1 degree. This means that when the vertical tails act as winglets, a significant amount of lift must be generated for them to be effective. The minimum drag case is for the wing, body, and vertical tail combination. The C_L where the minimum drag condition exists increases when the vertical tails are added. There is a second increase when the horizontal tails are added.

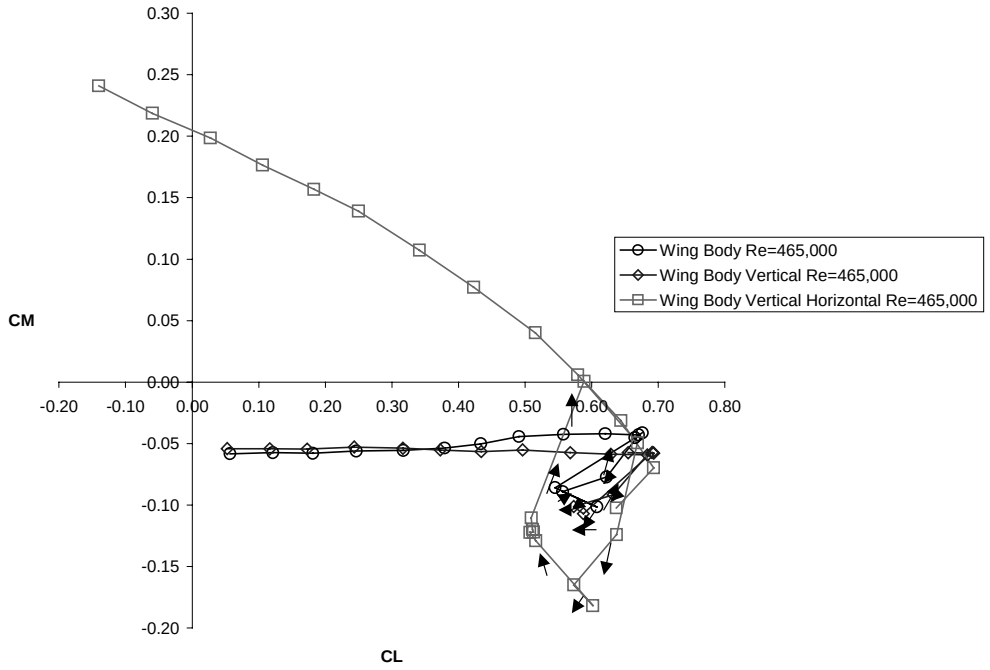

Figure 15: Small Model C_M vs. C_L with Configuration Changes (X_{ref}=10%$\overline{C}$)

The effects of model configuration on the pitching moment of the small model are shown in Figure 15. The model aerodynamic center is located in front of the moment reference position in the case with the wing-body alone with an aerodynamic center at 7% $\overline{C}$. This is shown by the slightly positive pitching moment slope. With the addition of the vertical tails, the aerodynamic center shifts slightly and is then behind the moment reference of ten-percent chord. The aerodynamic center goes to 11% $\overline{C}$ when the vertical tails are added. The addition of the horizontal tail creates a large nose-up pitching moment at zero lift and moves the aerodynamic center back to 42% $\overline{C}$. This large change in pitching moment may result from a slight misalignment when setting the horizontal tail to zero degrees of incidence relative to the centerline of the fuselage with no effort made to trim the model.

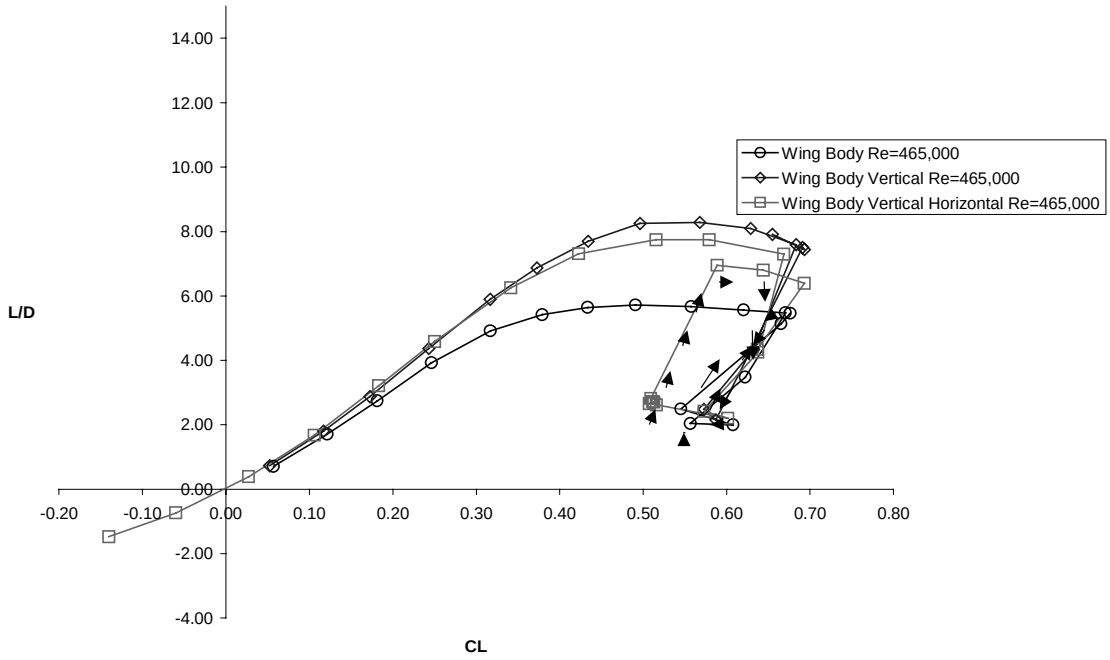

Figure 16: Small Model *L/D* vs. C_L with Configuration Changes

The *L/D* plot shown in Figure 16 provides a clear indication that the addition of the vertical tails improves the performance of the aircraft. The maximum *L/D* increases by 24% when the vertical tails are added to the wing-body combination. The maximum *L/D* is reduced with the addition of the horizontal tails by 6.5% from the maximum value. The *L/D* with the increased wetted area of the vertical and horizontal tails is still 16% greater than the value obtained for the wing-body alone. This effect could be mitigated with more consideration given to optimizing the horizontal tails.

The fact that the vertical tails are primarily reducing the drag rather than having a large effect on the maximum lift indicates they may be acting as winglets and providing a net thrust when introduced into the flow-field of the bodies. Optimizing the entire tail to act in concert as a winglet could make the increases on *L/D* much greater than this non-optimized case.

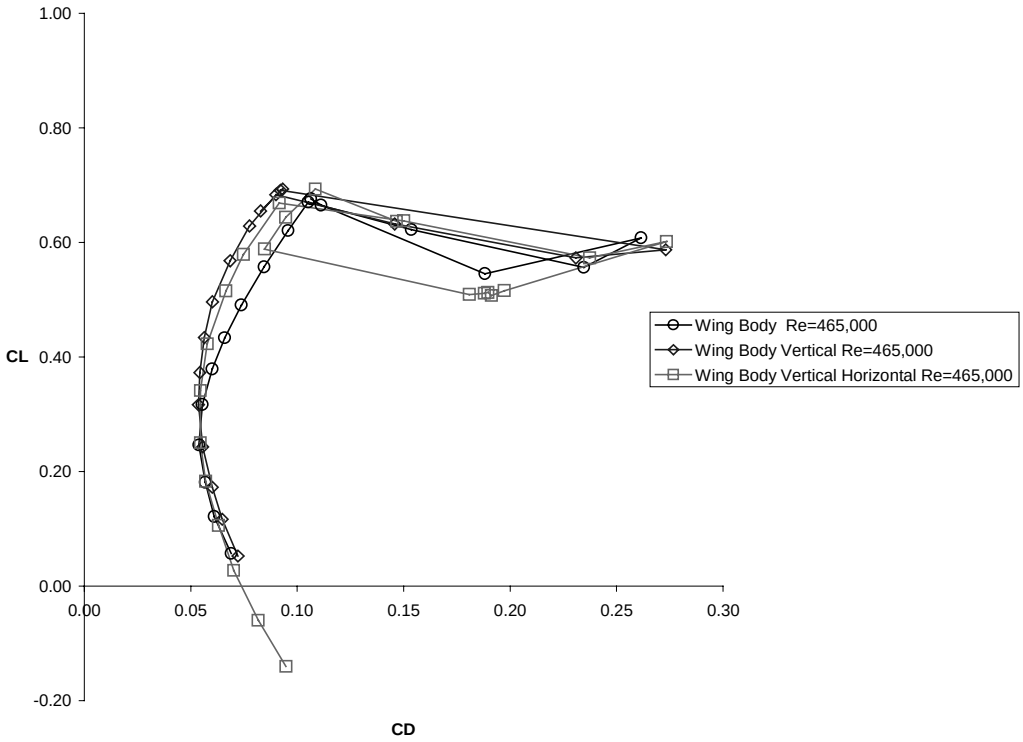

Figure 17: Small Model C_L vs. C_D with Configuration Changes

The drag polar for the small model is shown in Figure 17. This figure shows that the data for all configurations were similar when the C_L value dropped below 0.35. Above this value, the configurations with the vertical tails have less drag than the wing-body alone configuration. The C_L for L/D_{max} is approximately 0.6 for the wing-body, and vertical tail configuration.

Large Model Results

When reducing the data for the large model, blockage corrections were applied to all cases that had the bodies affixed to the wing. These corrections are described in Pope and Harper, 1966, pages 309 to 317 and detailed in Appendix II. They consist of two main corrections, one for the solid blockage of the air through the test section and another for wake blockage.

The moment head limits on the balance restricted the angle of attack range that could be used to obtain data to a maximum of 6 degrees. Without the moment head, a greater range of force data could be acquired before the force balance limits became a concern. It allowed the angle of attack to be increased to 14 degrees before the force limits were exceeded. This expansion in angle of attack range allowed stall to be reached with the wing and body combination.

Figure 18 shows that there was a slight Reynolds number dependence on C_L for the large model. The lower Reynolds number case was taken to an angle of attack of about 14 degrees. This stalled the configuration and the C_{Lmax} was 0.52.

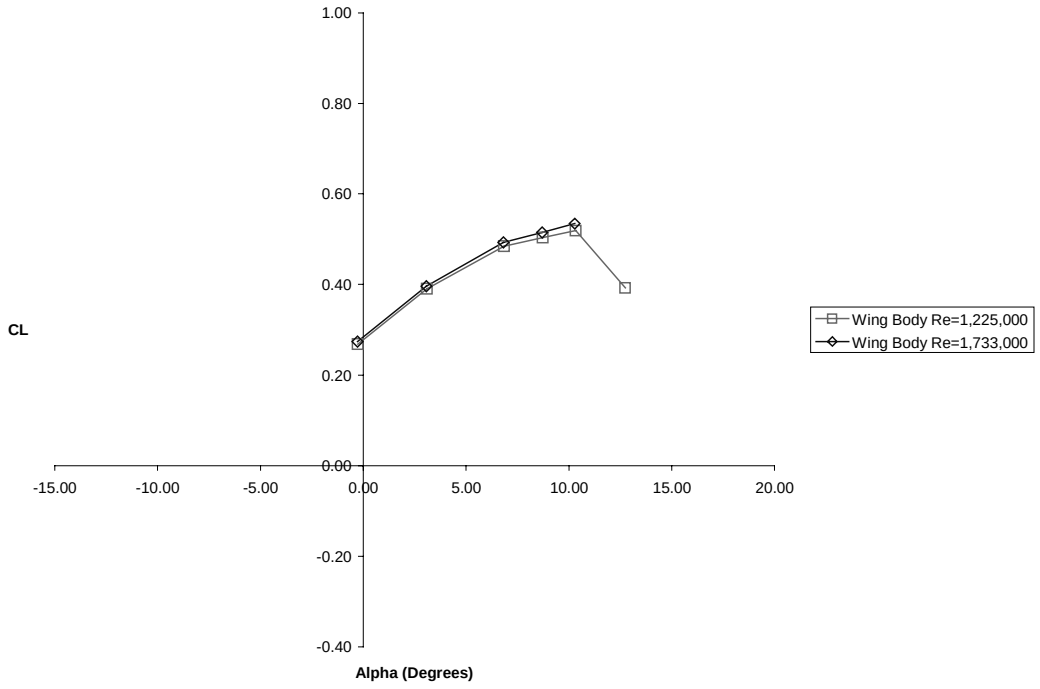

Figure 18: Large Model C_L vs. α at Different Reynolds Numbers (Angle of Attack Referenced to Body Centerline)

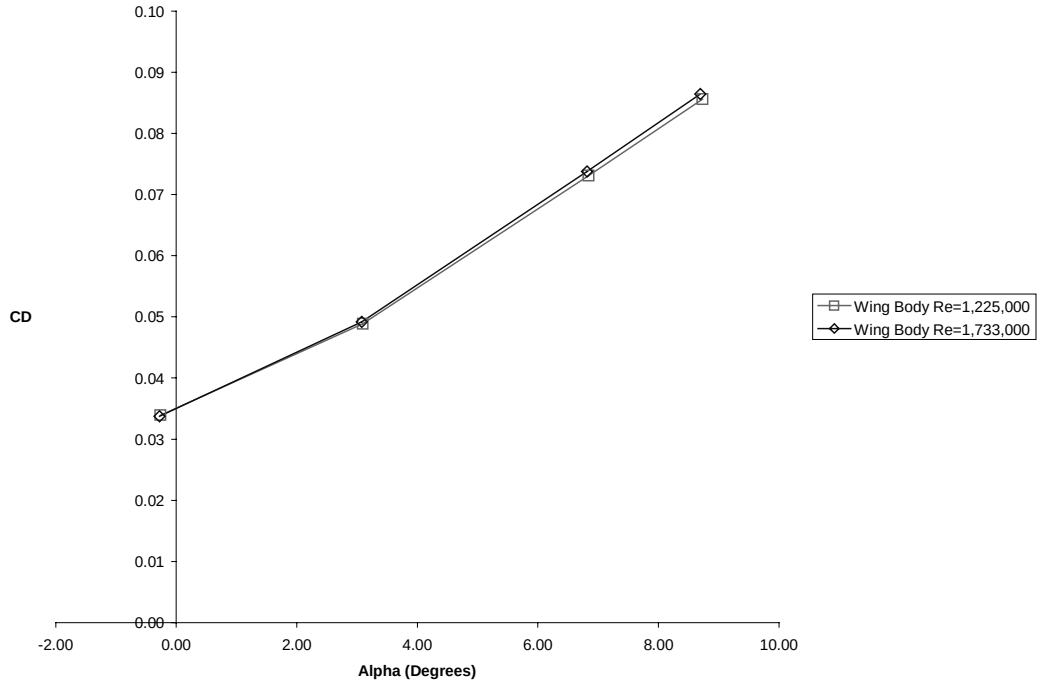

Figure 19: Large Model C_D vs. α at Different Reynolds Numbers (Angle of Attack Referenced to Body Centerline)

The drag coefficient data versus angle in Figure 19 shows a very slight reduction in drag with increased Reynolds. With further increases in Reynolds number it is possible that the minimum drag coefficient could continue to decrease. It is expected that the decreases would not be very large as the Reynolds numbers tested here are relatively high, and the difference over this range is slight.

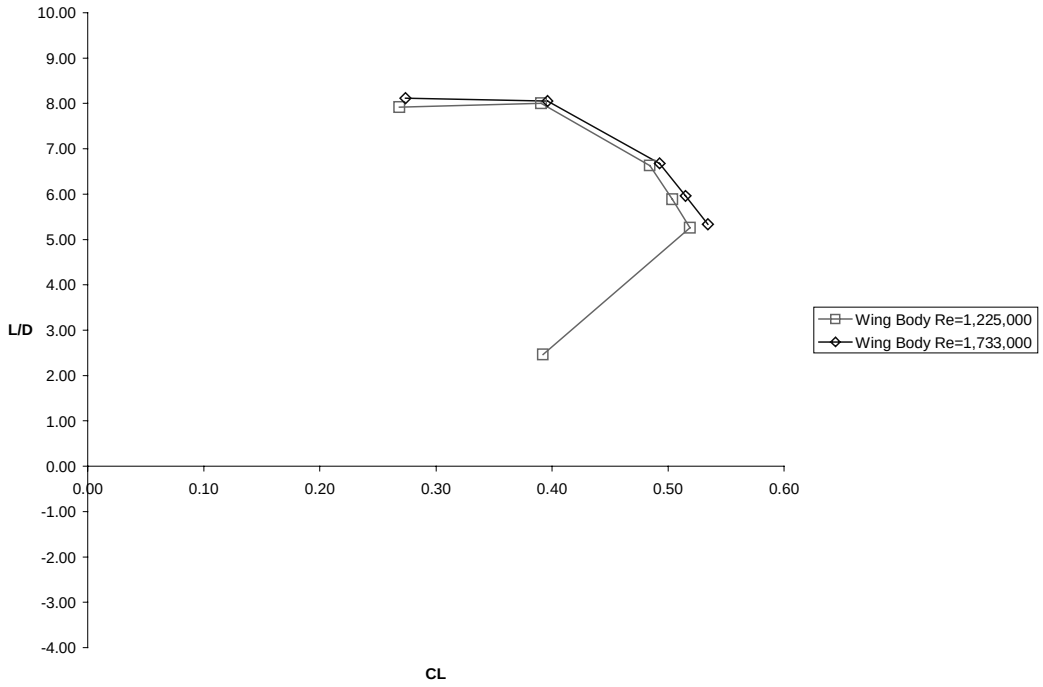

Figure 20: Large Model *L/D* vs. C_L at Different Reynolds Numbers

The *L/D* plot shown in Figure 20 shows that there is some increase in *L/D* for a given C_L with an increase in Reynolds number. This data also shows the maximum *L/D* is about 8.5, and it occurs at a C_L of approximately 0.45. This result again confirms the increase in the measured performance of the model with an increase in Reynolds number. This change is small, but noticeable.

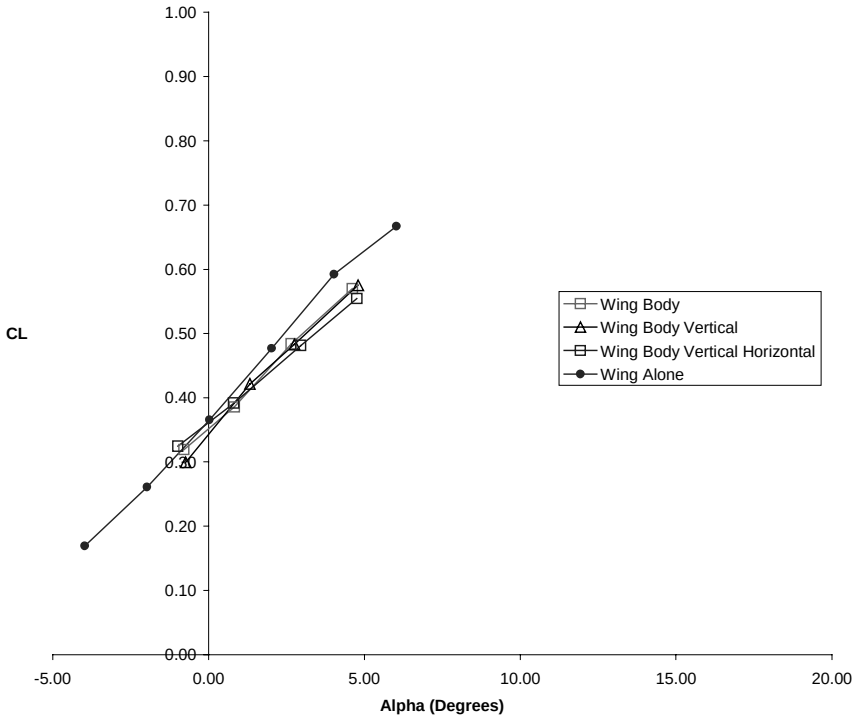

Figure 21: Large Model C_L vs. α with Configuration Changes (Angle of Attack Referenced to Body Centerline)

Figure 21 displays the effects on the lift data of adding the vertical and horizontal tail sections to the large model. This figure also shows the results of the wing alone tests. This test and all of the subsequent large model tests were performed at a Reynolds number of 1,225,000. The slope only changes slightly for all of the cases tested. The notable result is that the bodies decrease the lift curve slope when compared to the wing along. The lift curve slope increases when the vertical tails are added to the bodies. This change in slope with the addition of the vertical tails is more pronounced than that for the small model. The wing alone shows about the same lift at an angle of attack of zero degrees but a higher lift curve slope than the other configurations.

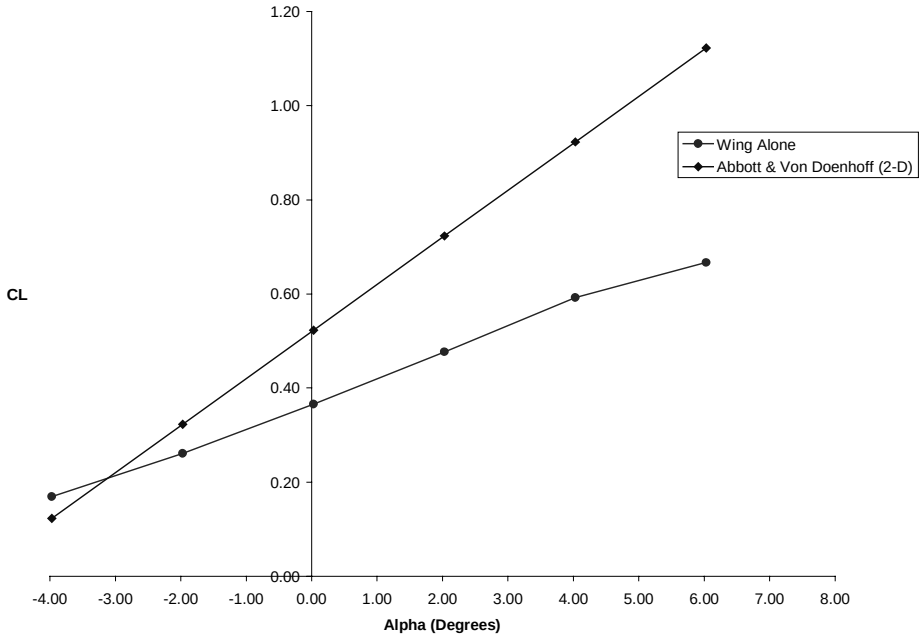

Figure 22: Large Model Wing Alone C_L vs. α Compared to Abbot and Von Doenhoff 2-D Data (Angle of Attack Referenced to Body Centerline)

Figure 22 shows the large model wing alone data compared with Abbot and Von Doenhoff 2-D data for the NACA 23012 airfoil section. This data shows that the slope of the three dimensional data is significantly lower then that of the two dimensional data. This is to be expected since the aspect ratio of the wing alone is only ~2. The zero lift angle of attack is also lower for the three dimensional data.

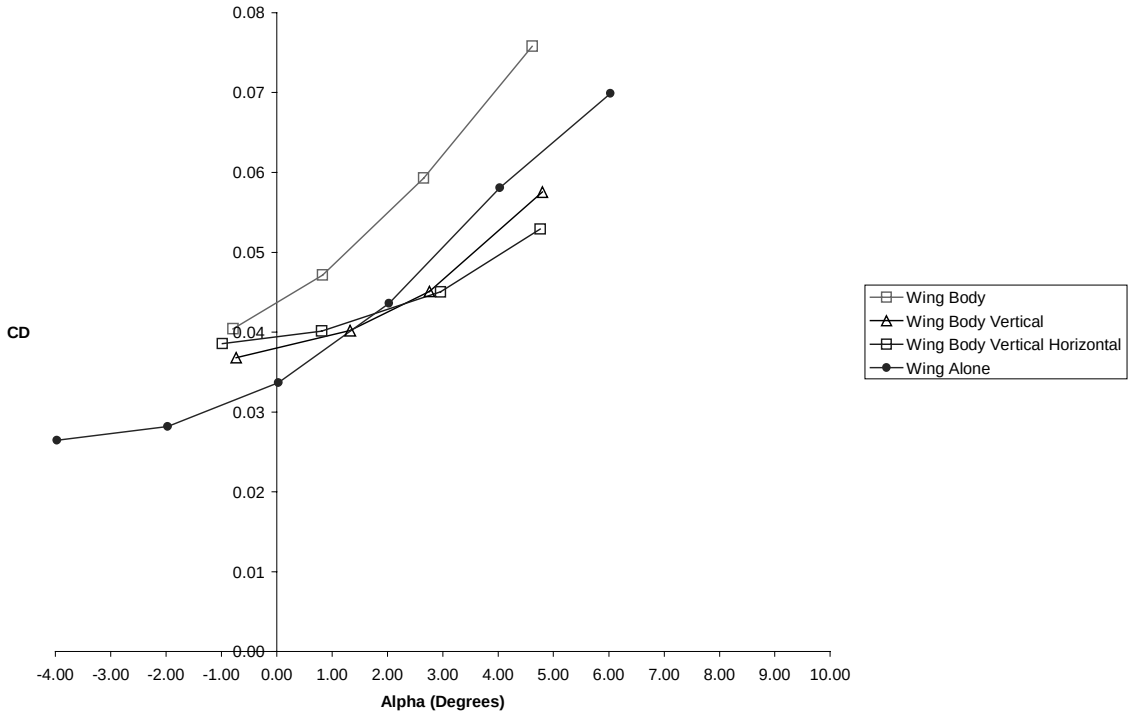

Figure 23: Large Model C_D vs. α with Configuration Changes (Angle of Attack Referenced to Body Centerline)

The drag data for the large model in Figure 23 shows that the wing alone has the minimum drag value over the range of α tested, and the wing body combination had the highest drag. The addition of the vertical tails reduced the minimum drag of the large model. This is the same effect that was observed for the small model and lends further weight to the idea that the vertical tails mounted on the aft bodies act as winglets and produce a net thrust. This effect is shown as the drag of the vehicle is reduced. Above an angle of attack of two degrees the drag is lower for the configurations with vertical tails then the wing alone. The wetted area is increased by 18% when the vertical and horizontal tails are added to the model. Even with this increase in wetted area the drag coefficient of the configuration is lower than the wing and bodies alone. When the horizontal tails are added to the model the drag is increased. Careful tailoring of the both the horizontal and vertical tails could make drag reduction even more significant.

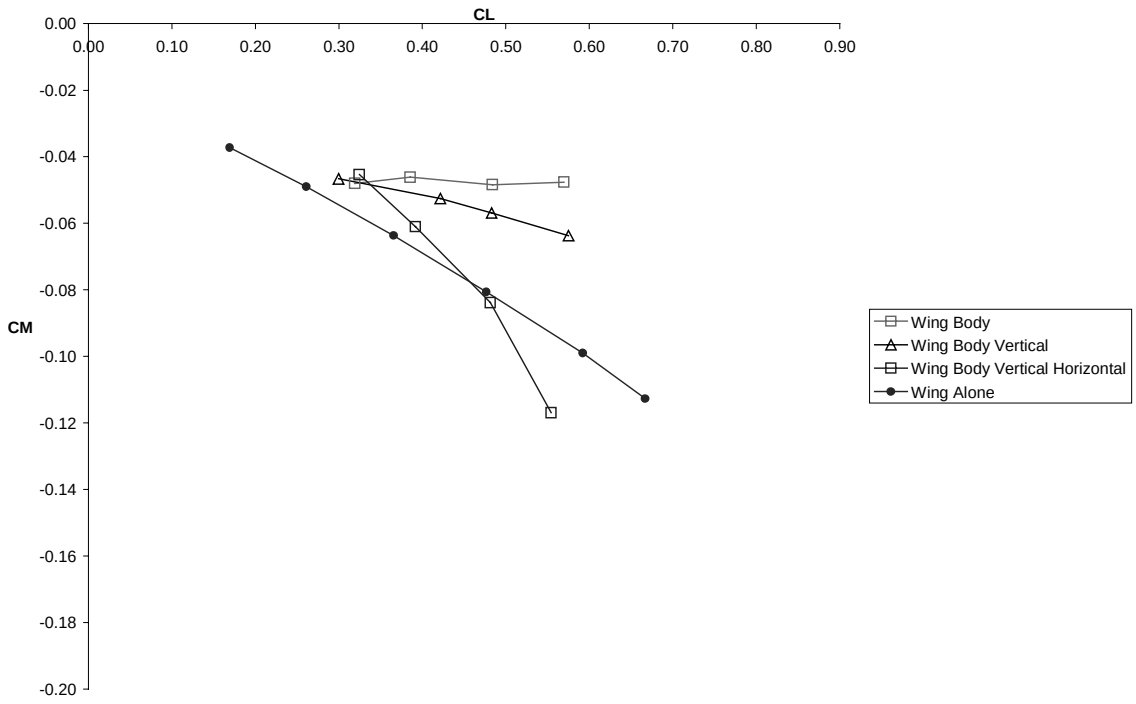

Figure 24: Large Model C_M vs. C_L with Configuration Changes (X_{ref}=10%$\overline{C}$)

The pitching moment data in Figure 24 shows that, as expected, the addition of the bodies to the wing is destabilizing. The moment curve slope is negative for the wing-alone case. The slope is nearly zero for the case with the bodies and wing. The addition of the vertical tails shifts the aerodynamic center further back. When the bodies are added they are destabilizing and shift the neutral point forward. The neutral point for the wing alone is at the 25.14%$\overline{C}$ location. The new neutral point location for the wing body combination is at 10.19%$\overline{C}$. The vertical tails move the neutral point to 16.19%$\overline{C}$. The horizontal tail has the effect of moving the neutral point a large amount to 40.45%$\overline{C}$.

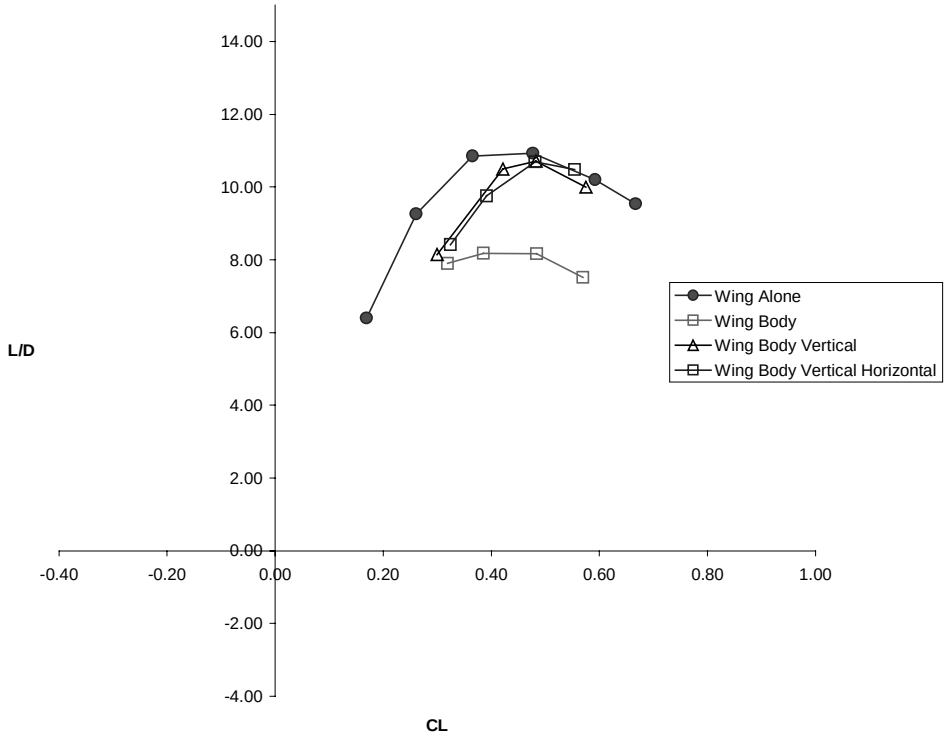

Figure 25: Large Model *L/D* vs. C_L with Configuration Changes

The *L/D* data in Figure 25 shows that the maximum *L/D* is obtained for the wing alone is 11.0. The worst case is the wing and body combination, which has a maximum *L/D* of 8.25. The addition of the vertical tails improves the L/D_{max} to 10.8, and the horizontal tails have little effect on the results with the L/D_{max} value again about 10.8. A substantial performance improvement was brought about with the addition of the tails. This is notable as the wetted area of the model is increasing substantially. However, the maximum *L/D* observed for the wing body and vertical tail is still fairly low when compared with optimized conventional configurations.

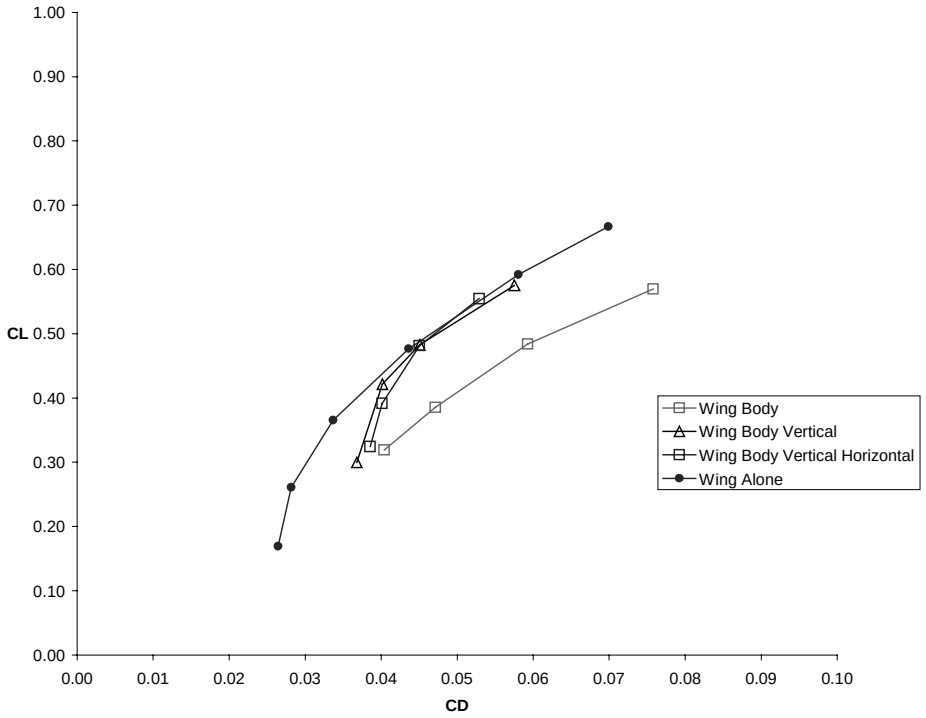

Figure 26: Large Model C_L vs. C_D with Configuration Changes

The large model drag polar is shown in Figure 26. This figure shows that the C_L for L/D_{max} is very close for the configurations with the vertical tails. The C_L for L/D_{max} is about 0.45 with the vertical tails added to the bodies. The data shows that the C_L values are very similar for the wing alone and cases with the vertical tails in a C_D range of 0.037 to 0.055. Above a C_D value of 0.04 the values for the wing alone case and the cases with the vertical tail are identical.

Large and Small Model Data Comparisons

Figure 27 shows the effects of vehicle configuration on lift data for both the large and small models. This data shows some disparity between the lift curve slopes for the different-sized models. The large model has a slightly higher slope, but a lower C_L for a given angle of attack with the addition of the vertical tails. The $dC_L/d\alpha$ value for the large model with the wing body and vertical tails is 0.042/deg, and the value for the small model is 0.032/deg. This could be a result of small geometrical differences between the handmade models. The large model does not exhibit the large change in zero lift angle of attack and lift curve slope that the small model does when the horizontal tail is added.

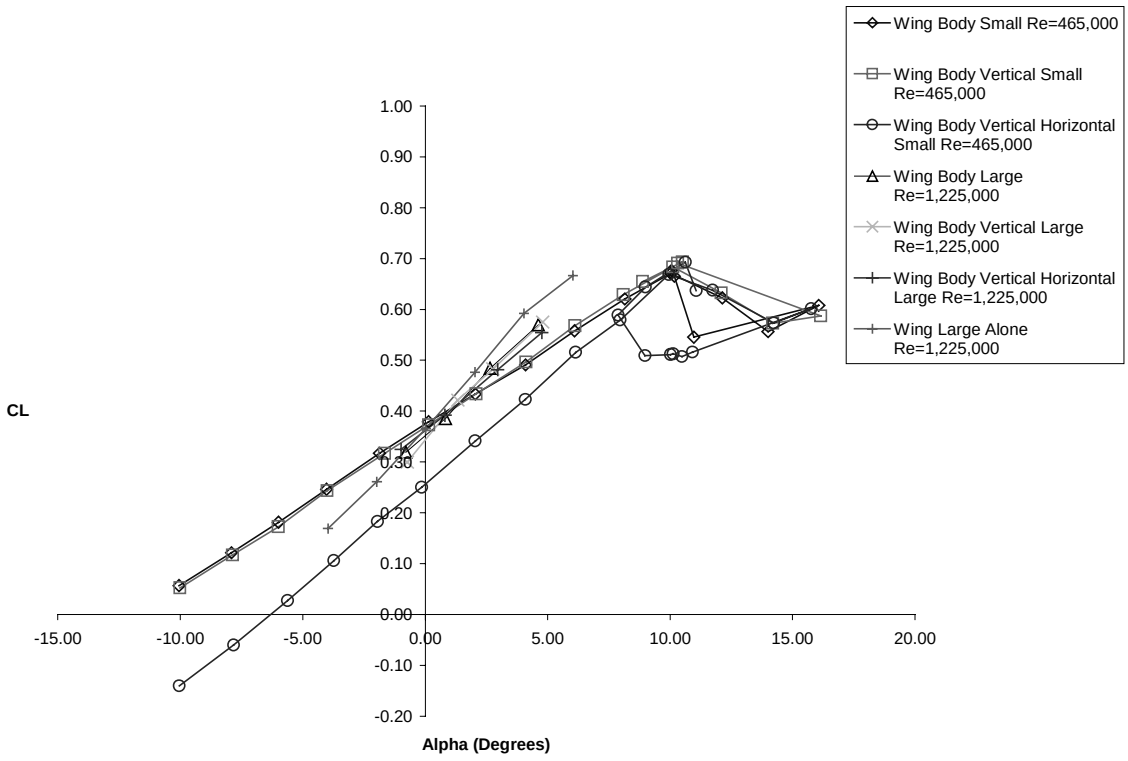

Figure 27: Large and Small Model C_L vs. α with Configuration Changes (Angle of Attack Referenced to Body Centerline)

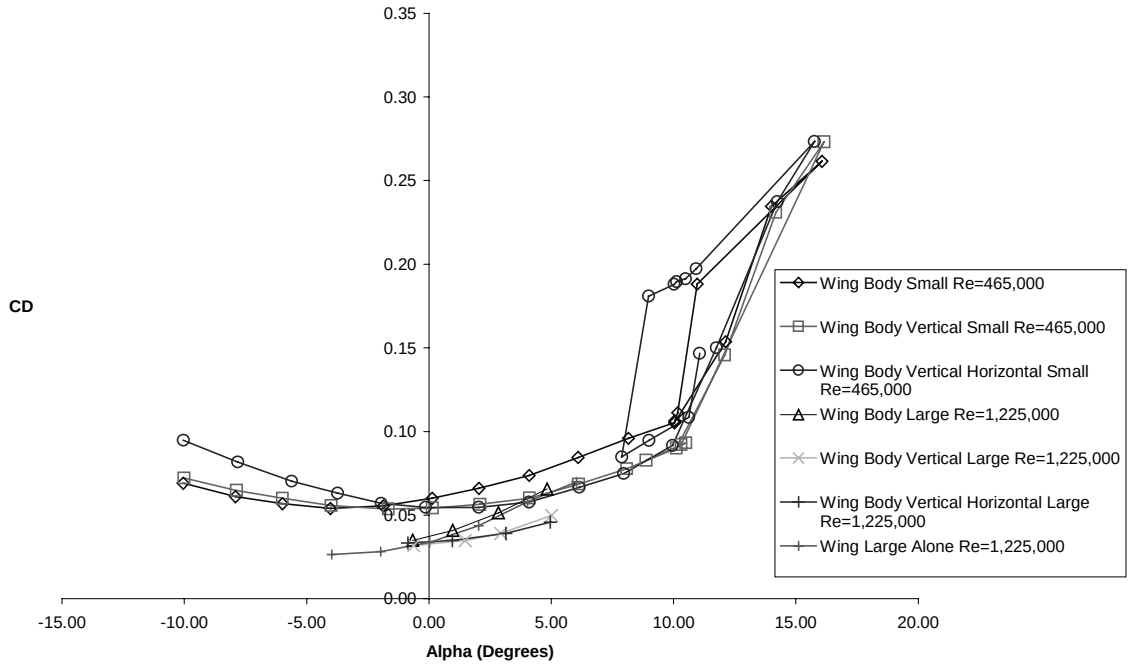

Figure 28: Large and Small Model C_D vs. α with Configuration Changes (Angle of Attack Referenced to Body Centerline)

Figure 28 compares the drag data of the large model to that of the small model. These data show that the large model has significantly lower drag coefficients than the small model at similar angles of attack. The effect of the higher Reynolds number is to reduce the measured drag coefficients due to the reduction of skin friction. For a flat plate, the skin friction coefficient would decrease by 16% with the same increase in Reynolds number as that from the small to large model. The models have up to a 38% change in the minimum C_D values so there is more then a simple Reynolds number effect.

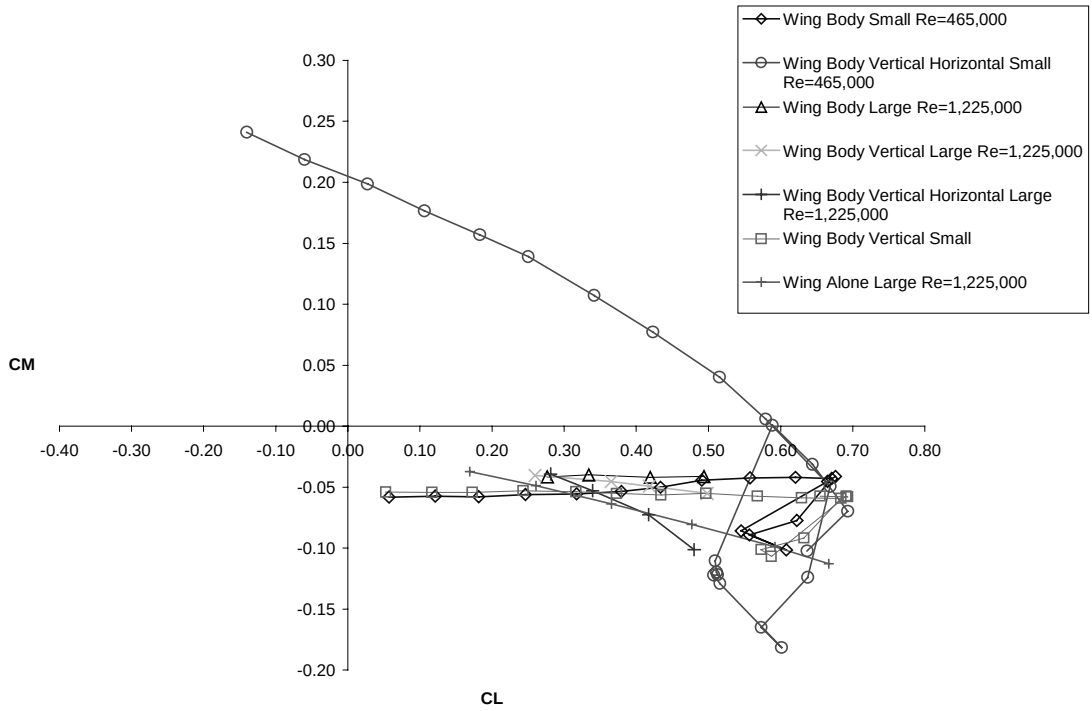

Figure 29: Large and Small Model C_M vs. C_L with Configuration Changes (X_{ref}=10%$\overline{C}$)

Figure 29 shows the pitching moment data for the large and small models. The data is in a similar range for the two models when looking at the slopes of the moment curves. This change is similar to that found for the small model with the horizontal tail affixed. The neutral points for both models are within 3% of each other for the full configuration. The zero lift pitching moment is significantly different between the large and small models; the intercept for the large model is 0.049 while that for the small model is 0.2091.

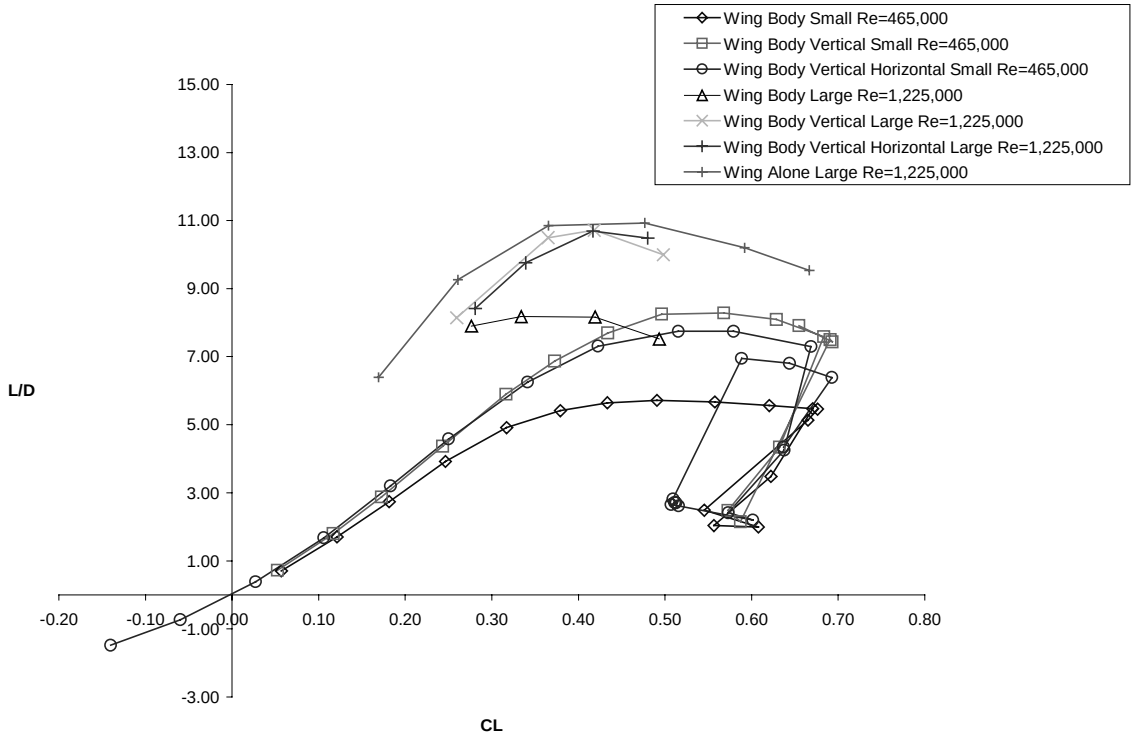

Figure 30: Large and Small Model *L/D* vs. C_L with Configuration Changes

The large model has a much higher maximum *L/D* then the small model in all configurations as shown in Figure 30. The addition of the vertical tails has a positive effect on the performance of both models. The large model, with its higher Reynolds number, exhibits better performance overall. The L/D_{max} for the wing and body combination is higher than the L/D_{max} for the wing-body and vertical tail combination of the small model. The large model achieves a maximum *L/D* of 10.7, and the small model exhibited a maximum of 8.5. The wing alone exhibited a maximum *L/D* of 10.9. The *L/D* decrease with the horizontal tails added is not as profound an effect for the large model as it was for the small model. This may indicate that the small model's horizontal tail was not aligned with the centerline of the fuselages or possibly the effects of the Reynolds number over that surface, which was quite low with a value of 154,000 increasing the drag of the tail.

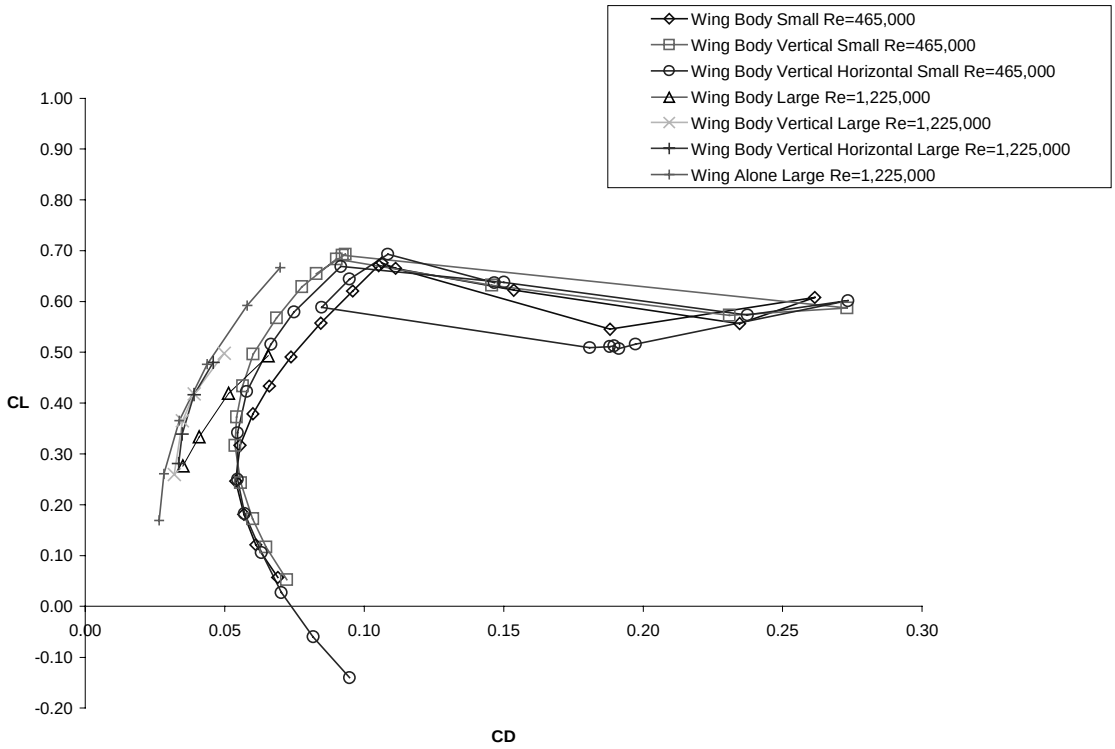

Figure 31: Large and Small Model C_L vs. C_D with Configuration Changes

The large and small model drag polar data is shown in Figure 31. The large model has a lower drag coefficient for a given lift coefficient. This translates into the higher L/D_{max} that was noted earlier. The small model has a C_{Do} value of about 0.07.

Flow Visualization Results

Extensive flow visualization experiments were performed to aid in interpreting the force and moment data. These tests consisted of using tufts mounted on the model and also tuft grids to view the flow in the wake. This flow visualization also aided in establishing the approximate core location of the vortices for use in later measurements.

The small model flow visualization test results are shown in Figures 32-34. All of these tests were performed between 49.8 *fps* and 86.3 *fps*. Figure 32 shows the model at a low positive angle of attack. The tufts on the end of the right body and on the tips of the vertical tails clearly show the presence of tip vortices. Figure 33 shows the same configuration viewed from above the test section of the tunnel. The tufts on the right body show angularity in the flow; the tuft at the top of the body is bent inward. A higher angle of attack test is shown in Figure 34 where the flow remains attached to the bodies, even when fully separated from the wing.

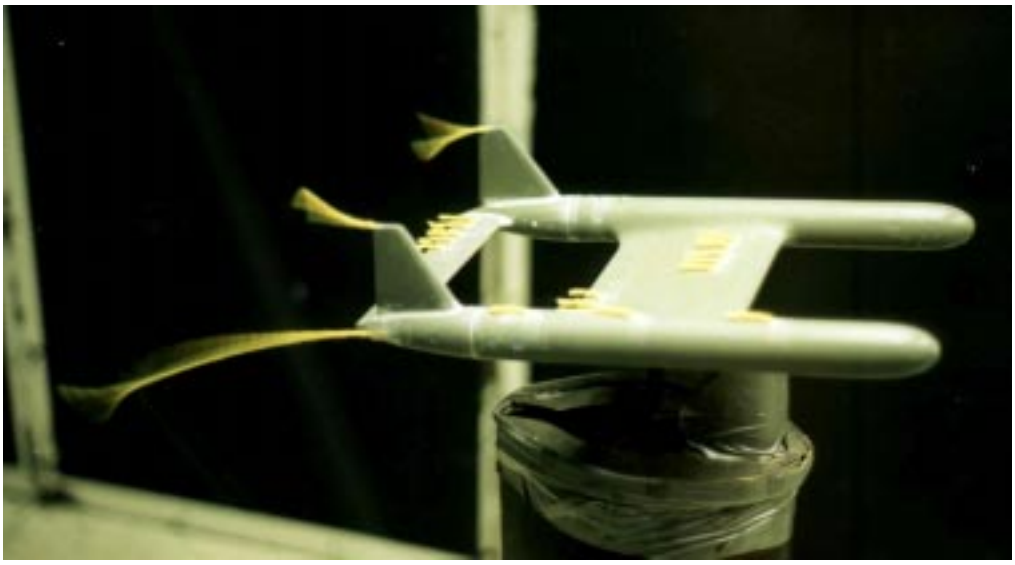

Figure 32: Small Model Tuft Test (Low AOA)

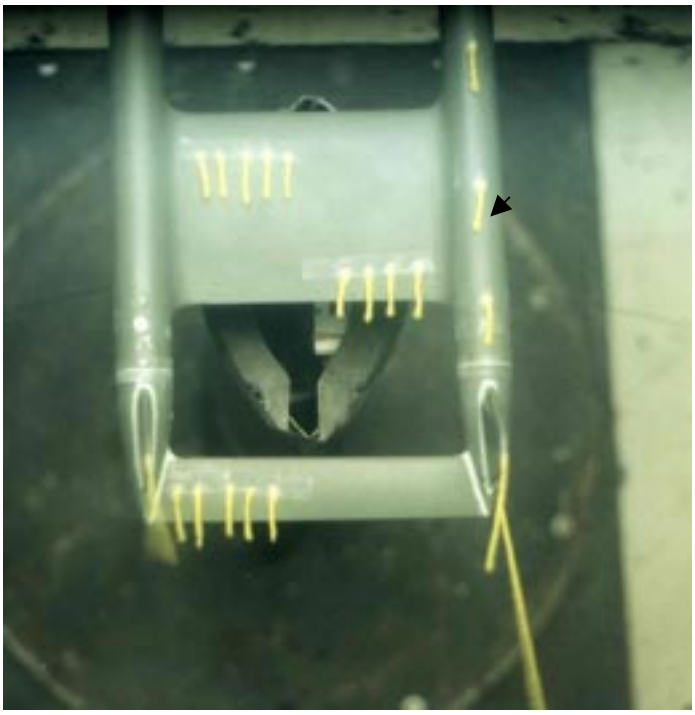

Figure 33: Small Model Tuft Test

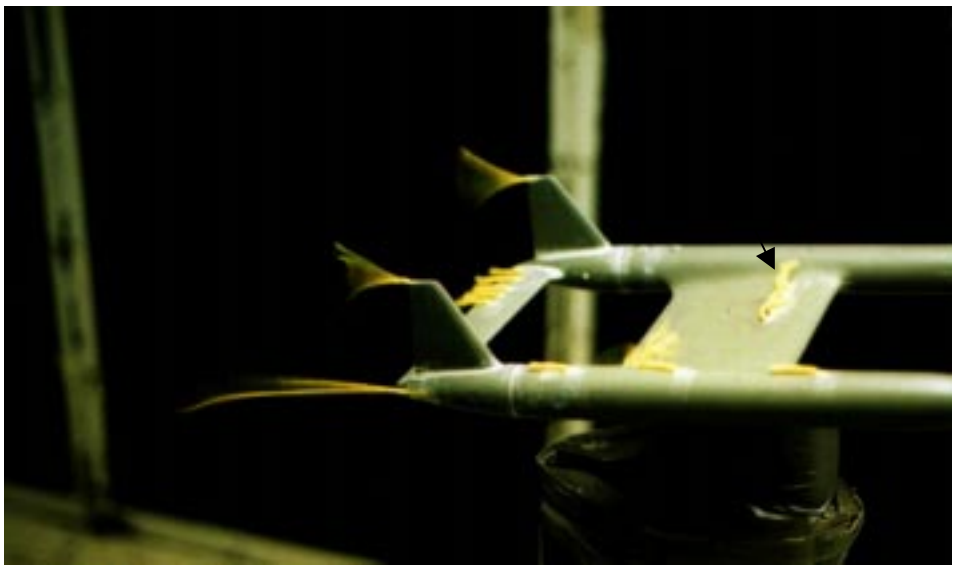

Figure 34: Small Model Tuft Test (High AOA)

Figures 35 and 36 are photographs of the tuft tests for the large model. The low angle of attack test in Figure 35 shows the flow attached on the entire model. When the angle of attack is increased, the flow separates at the wing centerline, and then progresses out to the bodies at the wing tips as seen in Figure 36. The flow on the bodies remains attached when the wing is stalled. This concurs with the results obtained for the small model.

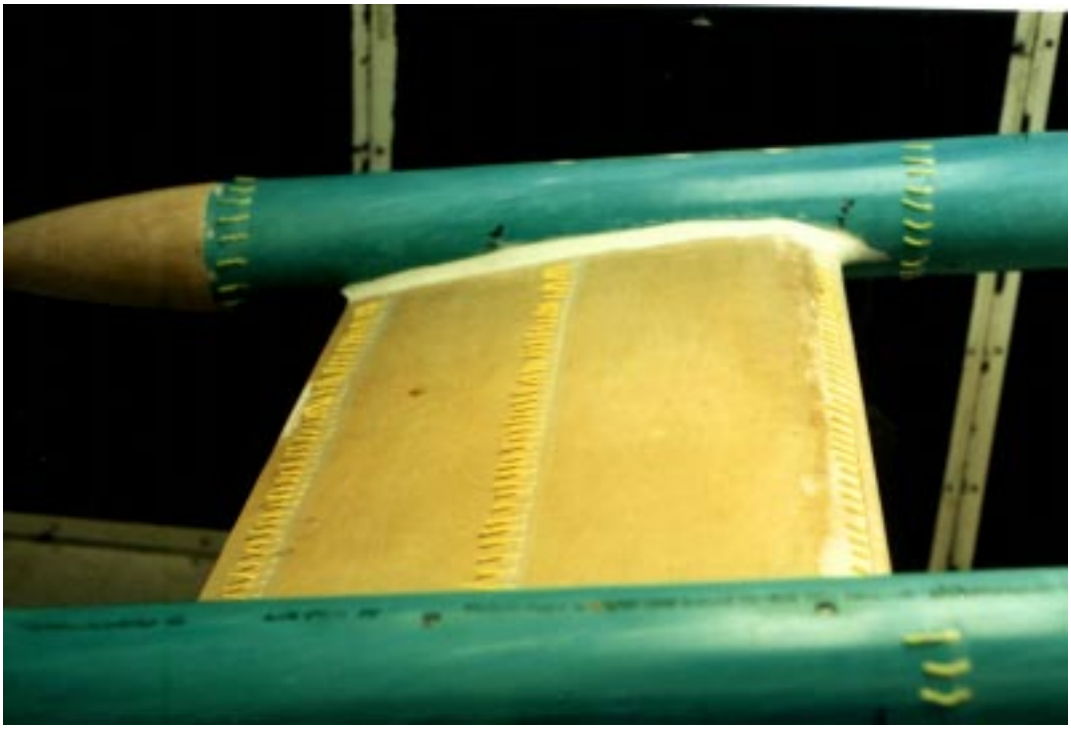

Figure 35: Large Model Tuft Test (Low AOA)

Figure 36: Large Model Tuft Test (High AOA)

Tuft grid testing aided in establishing the position and size of the trailing vortices, approximately two chord-lengths behind the model. The vortices can be seen in Figure 37 just outside the tail-cones of the model. Tuft grid tests were performed for the small model as well, but the results cannot be seen clearly in photos, as the vortices were quite small. The red arrows point to the approximate location of the vortex cores on the tuft grid.

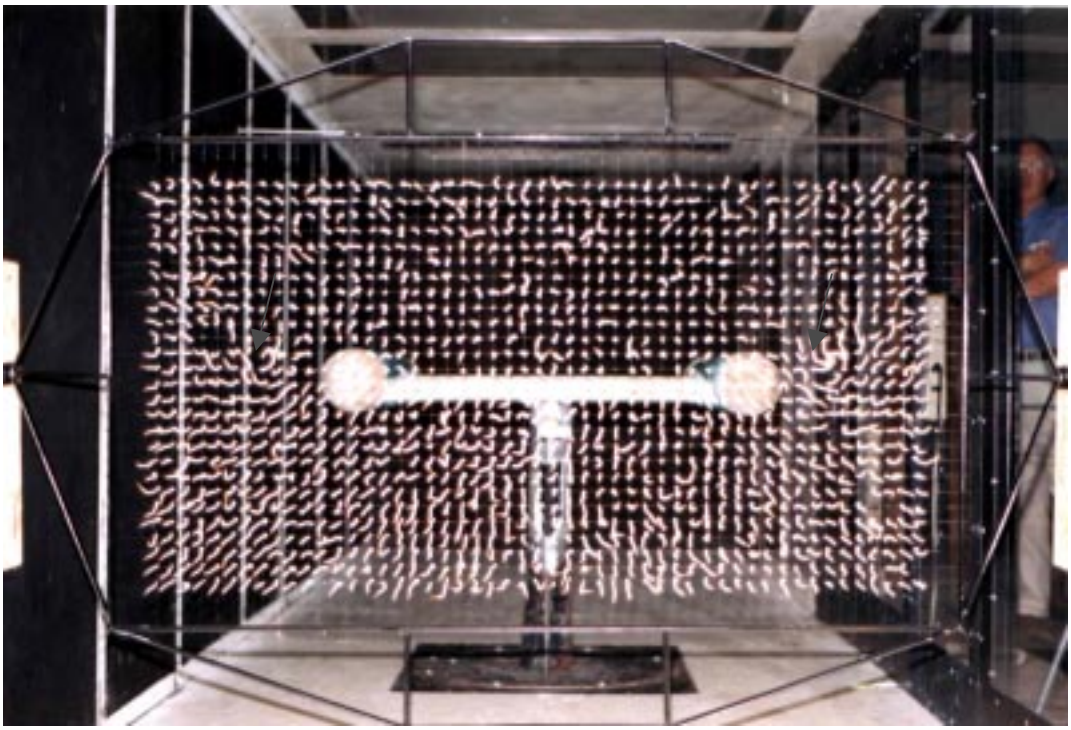

Figure 37: Large Model Tuft Grid Test

Analysis

VLM4.997 Vortex Panel Method

VLM4.997 was used to estimate the lift curve slope of the wing and body configuration. This method is described in Lamar 1982 and Margason 1971. The predicted $dC_L/d\alpha$ is plotted versus angle of attack and compared with the data for the large model, with bodies attached, in Figure 38. The slope obtained from VLM4.997 closely matched that obtained through the experiments with the large model. The $dC_L/d\alpha$ value for the wing and body obtained from experiment was 0.040, and the value predicted with VLM 4.997 was 0.046. The intercept for the VLM 4.997 prediction was selected to match the experiment data as the computer model used neglected camber.

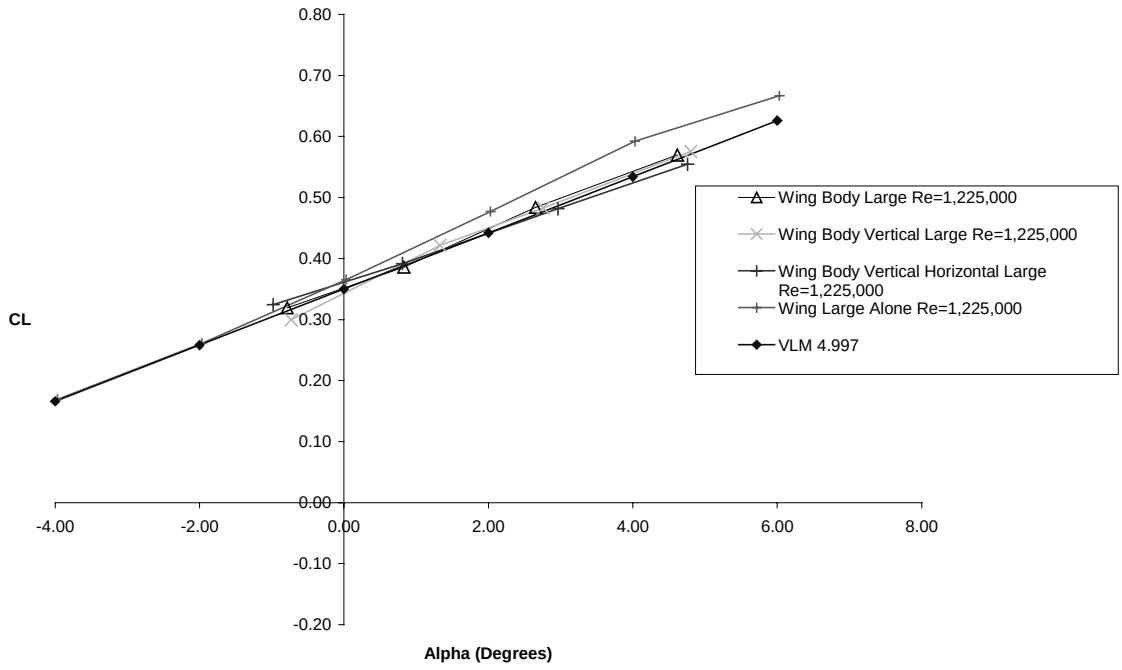

Figure 38: VLM4997 Compared with Large Model Experimental Data

Discussion

This investigation examined the aerodynamic behavior of an inboard wing configuration. The addition of the vertical tails, which appeared to act as winglets, reduced the drag of the configuration and increased the *L/D* substantially. The reduction in drag more then offset the increase in wetted area of the tail surfaces. The increased *L/D* of the large model indicates that there is some Reynolds number dependence on the results. Flow visualization confirmed the presence of the trailing vortices on both the large and small model. Vortices were observed from the trailing edge of the bodies and from the tips of the vertical tails.

Since the configuration tested was not optimized for maximum performance, the *L/D* was only moderate when compared with other transport configurations. Optimizing the configuration and designing the vertical tails to act specifically as winglets could yield a substantial increase in performance. The horizontal tail surfaces could be designed to act as winglets as well, further increasing the maximum *L/D*. This could be accomplished by angling the intersection of the body with the horizontal tails or changing their location slightly.

All of these results suggest areas for substantial improvement in aerodynamic performance. Natural Laminar Flow technology, boundary layer inlets, and engines mounted in the fuselages acting as tip mounted engines are all examples of technology. That could all be applied to this configuration achieving substantial performance gains.

References

Abbot , I.H., and Von Doenhoff, A.E., *Theory of Wing Sections*, Dover Publications Inc., New York, 1959

Lamar, J.E., and Herbert, H.E., *Production Version of the Extended NASA-Langley Vortex Lattice FORTRAN Computer Code*, -Volume I User's Guide, NASA TM83303, April 1982

Margason, R.J., and Lamar, J.E., *Vortex-Lattice FORTRAN Program for Estimating Subsonic Aerodynamic Characteristics of Complex Planforms*, NASA TN D-6142, February 1971

Pope, A. and Harper, John J., *Low-Speed Wind Tunnel Testing*, John Wiley & Sons Inc, New York, 1966

Spearman, M. L., "An Airplane Configuration with an Inboard Wing Mounted Between Twin Fuselages," AIAA 98-0440

Spearman, M. L., "A High-Capacity Airplane Design Concept Having an Inboard-Wing Bounded by Twin Tip-Mounted Fuselages," AIAA 97-2276

Appendix I

Tare values for the angle of attack changing device alone in the Stability Tunnel.

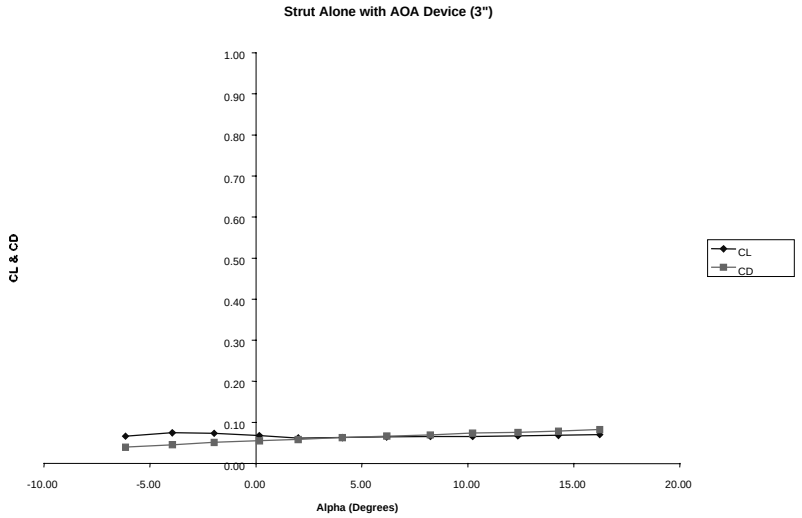

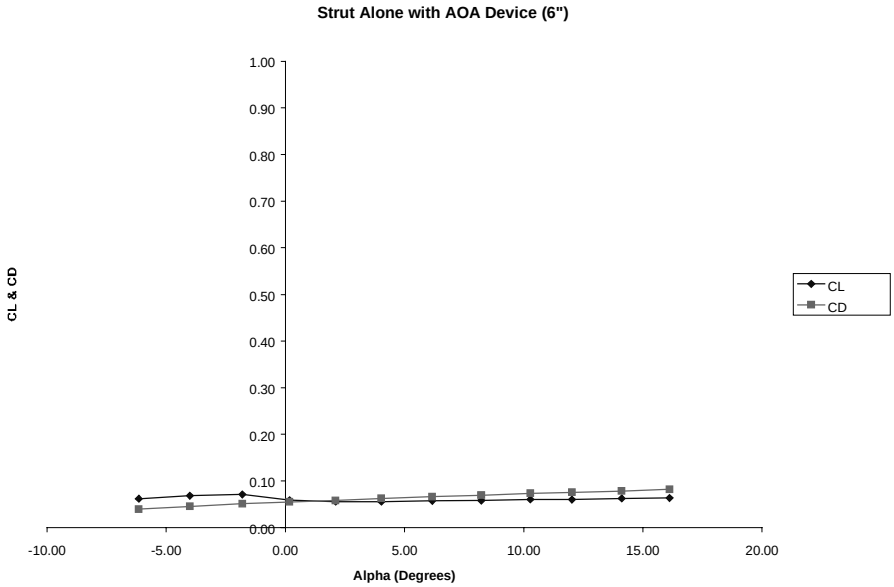

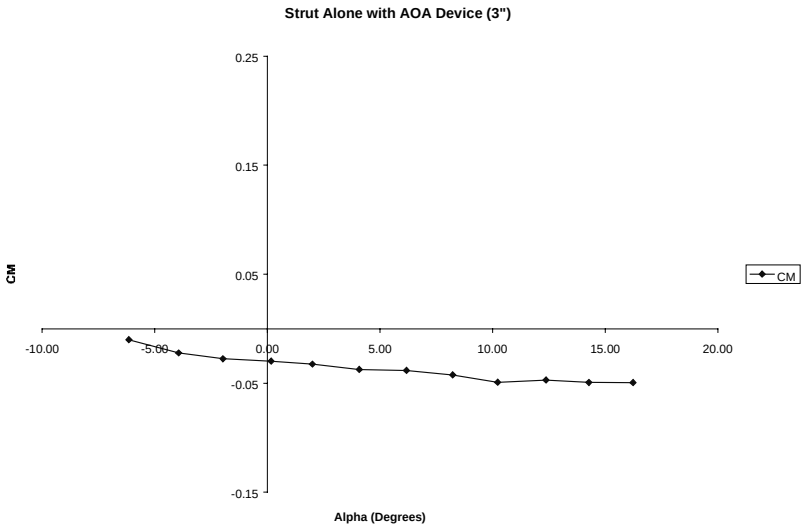
Strut Alone with AOA Device (3")
0.25
0.15
0.05
-0.05
-0.15
-10.00
-5.00
0.00
5.00
10.00
15.00
20.00
CM
CM
Alpha (Degrees)

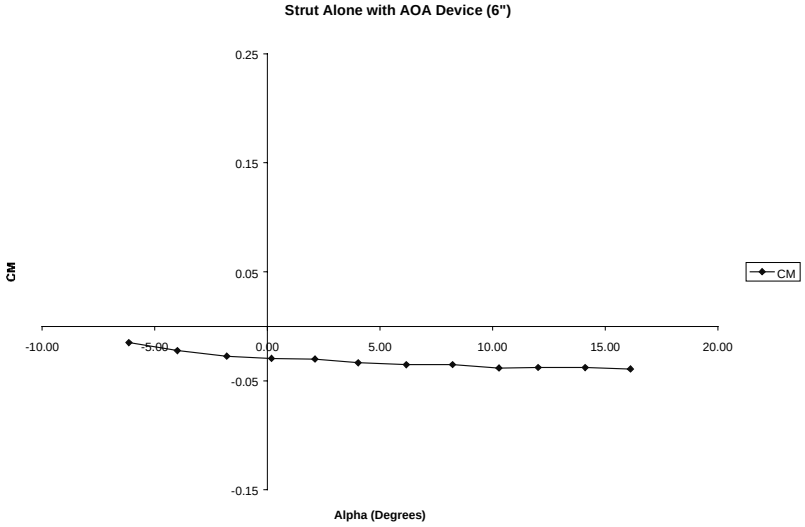
Strut Alone with AOA Device (6")
0.25
0.15
0.05
-0.05
-0.15
-10.00
-5.00
0.00
5.00
10.00
15.00
20.00
CM
CM
Alpha (Degrees)

Appendix II

Calculations of Blockage Effects

This section details the calculations used to correct the large model data for three dimensional boundary effects in a closed tests section. This was done as the model was large compared with the size of the tests section. The method used is given in more detail in Pope (1966, pages 320-369).

a= Lift Curve Slope

C= Tunnel Cross Sectional Area = 5256 in^3

C_{DU}= Uncorrected Drag Coefficient

C_{DoU}= Uncorrected Zero Lift Drag Coefficient

$\overline{C}$ = Wing Chord = 22.27 in

t/c= Thickness to chord ratio = 0.12

d/l= Fuselage Length/Diameter = 0.0917

W_v= Wing Internal Volume =1301 in^3

F_v= Fuselage Internal Volume = 2736 in^3

τ_1= 0.95

τ_2= 0.40

k= 0.5289

k_1=1

k_3= 0.97ϵ

δ= -0.14

λ=1

The following equations (1-3) are used to calculate a correction factor for the blockage of flow by the model in the tunnel. The blockage corrections consist of two distinct types. The first correction is represented by equation 2. This is the blockage due to the physical volume displaced in the tunnel and is know as solid blockage. The second type of blockage is due to the wake of the model. The correction factor for wake blockage is shown in equation 3. The sum of these two types of blockage results in the correction factor ϵ which is then used to correct the force and moment data.

$$\varepsilon = \varepsilon_{sb} + \varepsilon_{wb} \tag{1}$$

$$\varepsilon_{sb} = \frac{k_1 \tau_1 W_v}{C^{3/2}} + \frac{k_3 \tau_1 F_v}{C^{3/2}} \tag{2}$$

$$\varepsilon_{wb} = \frac{S_{ref}}{4C} C_{DU} \tag{3}$$

Equation 4 shows the corrections needed to find the true angle of attack of the model due to the changes in flow angle caused by blockage in the tunnel.

$$\alpha = \alpha_U + \left[\delta \frac{S}{C} C_L (57.3) \right] (1 + \tau_2) \tag{4}$$

Equations 5-8 describe the calculations necessary to correct the lift coefficient data for the wall effects.

$$\Delta\alpha = \Delta\alpha_1 + \tau_2 \Delta\alpha_1 \tag{5}$$

$$\Delta\alpha_1 = \frac{6\sigma}{\pi^2} C_l \tag{6}$$

$$\sigma = \frac{\pi^2}{48} \left(\frac{\overline{C}}{\sqrt{C}} \right)^2 \tag{7}$$

$$C_L = C_{LU} (1 - 2\varepsilon) - \tau_2 \Delta\alpha \cdot a \tag{8}$$

Equations 9-11 show the corrections for the drag coefficient data. Equation 9 calculates the drag coefficient change due to the blockage of the wing. The blockage effect of the

bodies is described by equation 10. Equation 11 shows all of the correction factors used to find the actual drag coefficient value.

$$\Delta C_{DW} = \frac{k_1 \tau_1 W_v}{C^{3/2}} C_{DU} \qquad (9)$$

$$\Delta C_{DB} = \frac{k_3 \tau_1 F_v}{C^{3/2}} C_{DoU} \qquad (10)$$

$$C_D = C_{DU}(1-2\varepsilon) - \Delta C_{DW} - \Delta C_{DB} + \delta \frac{S}{C} C_L{}^2 \qquad (11)$$

The moment correct was applied to the value of the moment at the quarter chord of the wing before it was transferred to the ten-percent chord value used in this report.

$$C_{M\,1/4} = C_{M\,1/4U}(1-2\varepsilon) + 0.25\tau_2 \Delta\alpha \cdot a \qquad (12)$$

The C_L data is shown in below in Figure AII-1. The main effect of the correction is a shift in angle of attack of one degree.

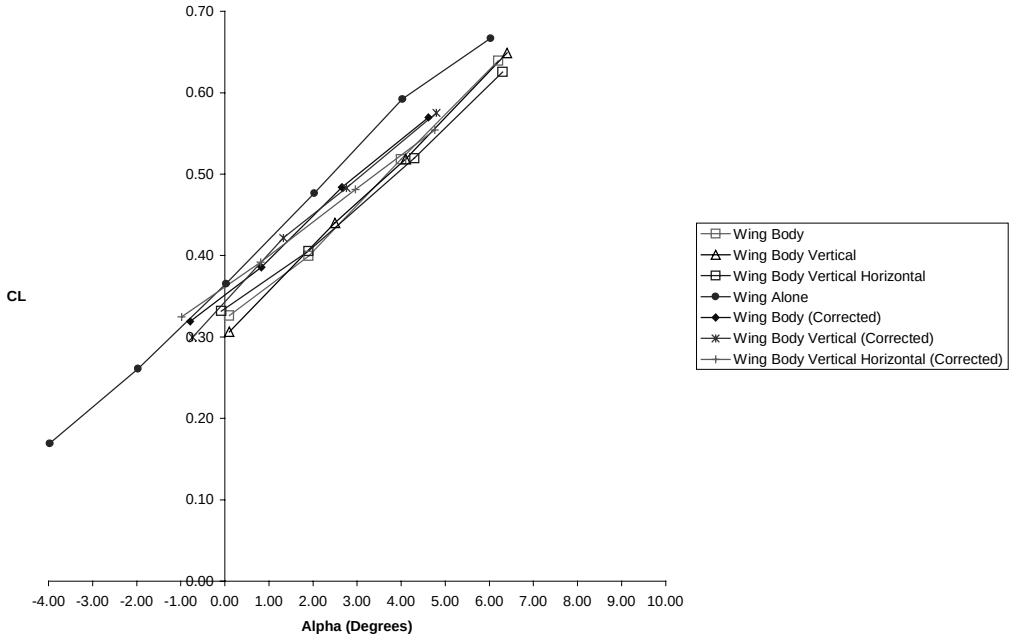

Figure AII-1: C_L Data Corrected and Uncorrected

VITA

Matthew W. Orr was born January 20, 1978, and he is the youngest of three sons of Marjorie and Marshall Orr. Interest in the design and construction of model aircraft lead to enrollment at Virginia Tech. Work with UAVs and a strong interest in flying were maintained throughout school. Graduation took place in December of 1999 with a Bachelor of Science degree in Aerospace Engineering with honors. A Ph.D. in aerospace engineering will be pursued.